KUNGL TEKNISKA HÖGSKOLAN

TRITA-MEK
Technical Report 1997:3
ISSN 0348-467X
ISRN KTH/MEK/TR—97/3-SE

A Study of Stability in AutoBalancing Systems using multiple Correction Masses

Jesper Adolfsson

Licentiate Thesis
Stockholm, 1997

Royal Institute of Technology
Department of Mechanics

A Study of Stability in AutoBalancing Systems using Multiple Correction Masses

Jesper Adolfsson
Department of Mechanics, Royal Institute of Technology
S-100 44 STOCKHOLM, Sweden

January 28, 1997

Abstract

The stability of an autobalancing system is investigated. This work is divided into three parts.

The first part is concerned with the stability in an isotropic two correction mass autobalancer. By isotropic it is meant that the system has the same stiffness and damping in the horizontal and vertical direction. It is shown that the equations of motion can be transformed, in the isotropic case, to a time independent form. This transformation reduces the complexity of the stability computations. The equilibrium positions are calculated. Linear stability analysis is done about these equilibriums. The influence of different parameters are investigated, such as the rotational speed, the suspension stiffness and damping, internal damping acting on the compensating masses and different mass configurations. It is shown that instability can occur when the rotational speed is above the natural frequency of the system. It is also shown that stability can depend on the amount of imbalance load in the system. When the internal damping acting on the correction masses is reduced, a super critical hopf bifurcation occurs.

The second part is concerned with the anisotropic autobalancer, i.e. with different stiffness and damping in horizontal and vertical directions. In this case the equations of motions are time dependant and stability analysis is performed by integrating the variational equations over one half period. It is shown that given enough separation in the horizontal and vertical natural frequency, regions of stability occur when the rotational speed is varied. It is also shown that some of the phenomena occurring in the isotropic autobalancer also occurs in the anisotropic autobalancer.

The third part studies the case when more than two compensating masses are used. This adds some complexity to the stability calculations since using three compensating masses gives a family of equilibrium positions. This means that the stability has to be calculated for all possible equilibrium configurations.

Contents

Chapter 1

Introduction

Autobalancing of rotating machines using moving correction masses is best accomplished where one wants to correct imbalanced rotation varying in time. The type of imbalance can be both static, dynamic or a combination of both. Depending on the design of the autobalancers continuously or discrete balancing can be achieved. The discrete balancing usually involves some sort of locking mechanism of the correction masses. The need of a locking mechanism is due to the fact that continuous balancing can only be achieved when certain system parameters are chosen correctly. The most noticeable system parameter, regarding continuous balancing, is the rotary speed.

The term auto in autobalancing refers to the fact that it is a passive system. By passive it is meant that no active forces are needed to move the correction masses. Therefore no controllers are needed in the system.

The idea behind autobalancers is old and the first patents are from the 1920's. There is not a widespread use of autobalance although there exist many different patents on the subject, mostly regarding the design of locking mechanism of the moving correction masses. Why autobalancers have not been used more widely depends on several things. For example the forces that move the correction masses to their proper location is small compared to the normal forces. The normal forces tend to be very high in practical applications which also require high surface finish and high precision in balance rings and correction masses. However this is not a serious obstacle since ball bearing manufactures have mastered these skills. It therefore seems that the most likely manufacturer of autobalancers will be the ball bearing industry. Another serious drawback is that it does not work at all rotary speeds, and this is here analyzed in greater detail. This means that for some systems, operating at rotary speeds which are not in the autobalancing regime, it is not possible to use this technique. In some system it might still be possible to use it with a locking mechanism of the correction masses. Locking mech-

anisms have been tested in turning lathes and stationary grinding machines. During normal operation the spindle is rigidly connected to the machine and the correction masses are locked. When imbalance occur one can release the spindle so it is suspended with springs. This allows the machine to enter the autobalancing regime and consequently the corrections masses are released. After autobalancing has occurred the correction masses are locked and the spindle is rigidly connected to the machine again. The locking mechanism is usually a mechanical device but other types exist. For example fluids with a melting point so that it is possible to have it solid when the correction masses are locked and melted when they move. The heating needed is usually accomplished by electrical means. Another important aspect of the problem is how system parameters should be chosen to achieve satisfactory autobalancing. It is commonly believed that the only criterion for autobalancing is that the rotary speed is above the natural frequency of system (see section 1.2 for an explanation). However this is not true in general and only appears to be one of several requirements on the system, as will be shown later. Theoretical studies in this field have been performed to prove this common misbelief. These theoretical studies, see for example V.I. Kravchenko *et al.*, see [2] [4] [3], have reached this conclusion by simplifying the problem. The nice thing about these studies is that they have obtained analytical results. With some heuristic reasoning one is lead to the same conclusion (see section 1.2).

Autobalancers have successfully been used in grinding machines, such as the Atlas Copco Grinder GTG 40 equipped with an SKF Auto-Balancing Unit. Imbalance occur in grinding machines because of wear. This installation has reduced vibration levels to less than half of the vibrations occurring without the autobalancing unit. This means that the operator now can use the grinding machine without time restrictions. Other successful attempts have been washing machines where the load causes imbalance during spin drying. This has been tested, with good result, by Wascator in their commercial washing machines. Other areas where it has been tested with various results are refrigerator compressors to reduce noise from piston movements, fans operating in environments where dirt attaches to the blades such that when the dirt comes imbalance occurs.

1.1 Objectives

This work is mainly focused on how different parameters influence the autobalancing system. In previous work by the author, see [1] it is shown that a relatively simple analytical model accurately models a real autobalancing system. This was accomplished by numerical simulations and measurements

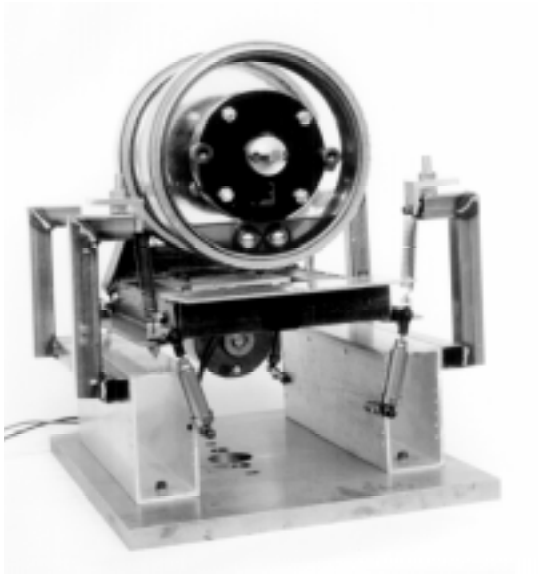

Figure 1.1: Picture of the experimental machine. The suspension is similar to a washing machine suspension. Two balance rings can be fitted on the axis of rotation. The correction masses are ballbearing balls.

on an experimental autobalancer built by the author, see picture 1.1. Since the model accurately describes the real system, stability analysis are made on the equations of motion. Calculations are performed on a plane isotropic and anisotropic two-ball balancer. In the last chapter it is shown how calculations on an autobalancer equipped with more than two balls can be made. Equations of motions are linearized and eigenvalues and eigenvectors are calculated about the equilibrium positions. Also normal form calculations are performed to analyze hopf bifurcations.

While working on the experimental machine a self sustained oscillation of the ball bearing balls, about their equilibrium position was found. This was not possible to explain with previous stability analysis. However, it will later be shown that these oscillations can be predicted by analytical/numerical means.

1.2 Illustrative model

There are two common designs of autobalancers. The most common design is letting balls move in a circular ring centered about the axis of rotation. This ring is usually filled with some viscous media such as oil. It will be shown

later that choosing the right viscosity is of major importance to achieve good performance. This construction is used in the GTG 40 grinding machine mentioned above. The second design is to use pendulum arms mounted on the axis of rotation. This design has been used in turning lathes. There also exist autobalancers where the moving correction masses are small carriages with wheels mounted on them. The reason for using carriages is that it can be designed with a better weight to occupied volume ratio, therefore reducing the volume of the balance rings compared to ball balancers. However, the carriage is a more complex design compared to using balls and is therefore not widely used. However in respect to the models used in this work these designs are mechanically equivalent and can be modelled with the same analytical model.

To get an idea of how autobalancing works consider figure 1.2. Assume that the system has low damping compared to the critical damping (for an introduction to basic theory of vibration see for example Thomson, Theory of Vibration with Applications [7]). The behavior to exploit is that we will have a π phase shift when the rotary speed is above the natural frequency of the system.

When the driving angular velocity ω of the system is below the natural frequency of the system we will have zero phase shift between the line AB and BC in figure 1.2. The natural frequency of the system is here defined as

$$\omega_n = \sqrt{\frac{k}{M + m + \sum_{i=1}^{n} m_i}}. \tag{1.1}$$

where M is the system mass and m is the mass of the unbalanced component and m_i is the mass of the i'th compensating mass. If m and the m_i's are small compared to M the expression for the natural frequency reduces to the normal expression $\omega_n = \sqrt{k/M}$. A small mass on a ring centered about the axis of rotation B would then move, as indicated in the figure, to the same side as the unbalance. This would increase the amplitude, line AB thus making the vibrations worse. However, when the system rotates at speeds above the natural frequency of the system we will have a π phase shift between the line AB and BC. A small mass, positioned the same way as before, would then tend to the opposite side of the unbalanced component. Assuming that this quasi static argument holds and that there are at least two masses moving symmetrically about the line BC the amplitude AB would decrease. In this quasi static argument it is assumed that the damping is small compared to the critical damping, which implies a phaseshift of π radians when ω goes from just below to just above the natural frequency. It is also assumed that there are no inertial forces due to the compensating masses acting on the system.

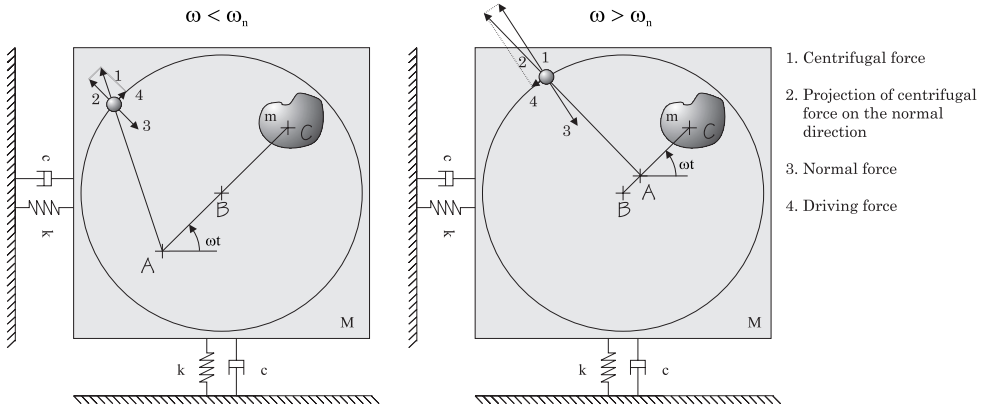

Figure 1.2: Figure showing the direction the centrifugal force would move a small imaginary mass on a ring when angular velocity is below and above the natural frequency of the system.

If more damping where present this phase shift would occur through a large region and this analysis would fail since it would not be clear what would happen when ω is in the range around ω_n.

Chapter 2

Analytical model

2.1 Derivation of equations of motion

To investigate the dynamics of autobalancing an analytical model constrained to move in a plane is used. This might appear to be a serious constraint since in most autobalancers the static unbalance is not situated in the same plane as the autobalancer. However, when using a one plane auto balancer one is forced to place the autobalancer as close as possible to the plane of unbalance. Therefore the plane analytical model will closely resemble an actual system, such as a grinding machine equipped with an autobalancer. If it is not possible to put the auto balancer in the plane of static unbalance or if you have dynamical unbalance one could use two auto balancers, letting the static or dynamic unbalance be situated anywhere between the autobalancers. This setup is for example used in washing machines. Actually it is possible to let the plane of static unbalance be situated outside the auto balancers.

In this model (see figure 2.1) the mass M is able to move in the $\mathbf{n_1}$ $\mathbf{n_2}$ plane. Linear springs and a linear viscous dampers are attached to mass M. Springs are considered to work in orthogonal directions to each other, the same applies to the dampers. The springs equilibrium position is the point A, therefore the displacement of mass M is measured from A to B with coordinates x_1 along $\mathbf{n_1}$ and x_2 along $\mathbf{n_2}$. The rotating mass is divided into two parts, the mass M with centre of mass at B and the mass m with centre of mass at C situated a distance e from B. The point C is assumed to be rotating about the geometrical centre B with angular velocity ω. The compensating masses, with mass m_i and rotational inertia i_i, are assumed be rotating, without slipping, on a circular path centered about the geometrical centre B. The distance from B to the centre of mass of the compensating mass is l_i and the radius of the compensating masses are r_i. The angular

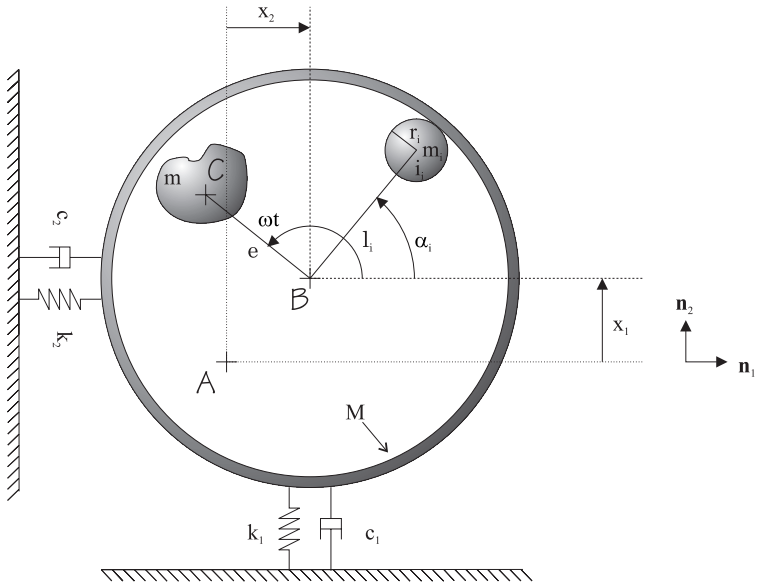

Figure 2.1: The auto balancing model.

coordinate is α_i. The forces acting on the compensating masses are assumed to linear in their relative speed compared to the rim. The viscous damping acting on the correction masses will be referred to as internal damping. The viscous damping from dampers will be referred to as external damping. The derivation of the equations of motion was made in Sophia, see [5]. Sophia is a set of routines for doing mechanics in computer algebra packages, such as Maple and Mathematica. Sophia was developed by Professor Martin Lesser at KTH. The equations of motion are

$$M'\ddot{x}_1 + c_1\dot{x}_1 + k_1 x_1 = me\omega^2\cos(\omega t) + \sum_{i=1}^{i=n} m_i l_i(\ddot{\alpha}_i \sin(\alpha_i) + \dot{\alpha}_i^2\cos(\alpha_i)), \quad (2.1)$$

$$M'\ddot{x}_2 + c_2\dot{x}_2 + k_2 x_2 = me\omega^2\sin(\omega t) + \sum_{i=1}^{i=n} m_i l_i(\ddot{\alpha}_i \cos(\alpha_i) - \dot{\alpha}_i^2\sin(\alpha_i)), \quad (2.2)$$

$$(m_i + \tfrac{I_i}{r_i^2})l_i\ddot{\alpha}_i + l_i(\delta_i + \tfrac{\gamma_i}{r_i^2})(\dot{\alpha}_i - \omega) = m_i(\ddot{x}_1\sin(\alpha_i) - \ddot{x}_2\cos(\alpha_i)) \quad (2.3)$$
$$i = 1, \ldots, n,$$

where M' equals $(M + m + \sum_{i=1}^{n} m_i)$ and is introduced since it occurs frequently. Parameter m is superfluous since the masses M and m are rigidly connected. It is introduced since parameter analysis will be simplified by it.

Chapter 3

The isotropic case

3.1 Derivation of equations

The isotropic case, where k_1 equals k_2 and c_1 equals c_2 is interesting since it is possible to get the equations of motion in a time independent form. An example of a isotropic system could be an autobalancer mounted on a rotating shaft, where the shaft is stiffly mounted. To get the equations in a time independent form is accomplished by expressing the position of point B relative to the point A with coordinates along the axis $\mathbf{a_1}$ and $\mathbf{a_2}$ (see figure 3.1). It can be expressed as a substitution

$$x_1 = q_1 \cos(\omega t) - q_2 \sin(\omega t) \quad , \tag{3.1}$$

$$x_2 = q_1 \sin(\omega t) + q_2 \cos(\omega t) \quad , \tag{3.2}$$

$$\alpha_i = \beta_i + \omega t \ , \ i = 1, \ldots, n. \tag{3.3}$$

inserted into equations 2.1,2.2,2.3. Furthermore, since equations 2.1 and 2.2 are the projections of the time derivative of the linear momentum along $\mathbf{n_1}$ and $\mathbf{n_2}$ we now need the projections along $\mathbf{a_1}$ and $\mathbf{a_2}$.

This is easily accomplished in Sophia since it has the ability to express vectors in all defined reference frames. The time independent equations can be written as

$$\begin{bmatrix} M' & 0 \\ 0 & M' \end{bmatrix} \begin{bmatrix} \ddot{q}_1 \\ \ddot{q}_2 \end{bmatrix} + \begin{bmatrix} c & -2\omega M' \\ 2\omega M' & -c \end{bmatrix} \begin{bmatrix} \dot{q}_1 \\ \dot{q}_2 \end{bmatrix} +$$

$$\begin{bmatrix} k - \omega^2 M' & -c\omega \\ c\omega & k - \omega^2 M' \end{bmatrix} \begin{bmatrix} q_1 \\ q_2 \end{bmatrix} = \begin{bmatrix} me\omega^2 \\ 0 \end{bmatrix} + \tag{3.4}$$

$$\sum_{i=1}^{n} m_i l_i \left(\begin{bmatrix} \ddot{\beta}_i & (\dot{\beta}_i + \omega)^2 \\ (\dot{\beta}_i + \omega)^2 & -\ddot{\beta}_i \end{bmatrix} \begin{bmatrix} \sin(\beta_n) \\ \cos(\beta_n) \end{bmatrix} \right)$$

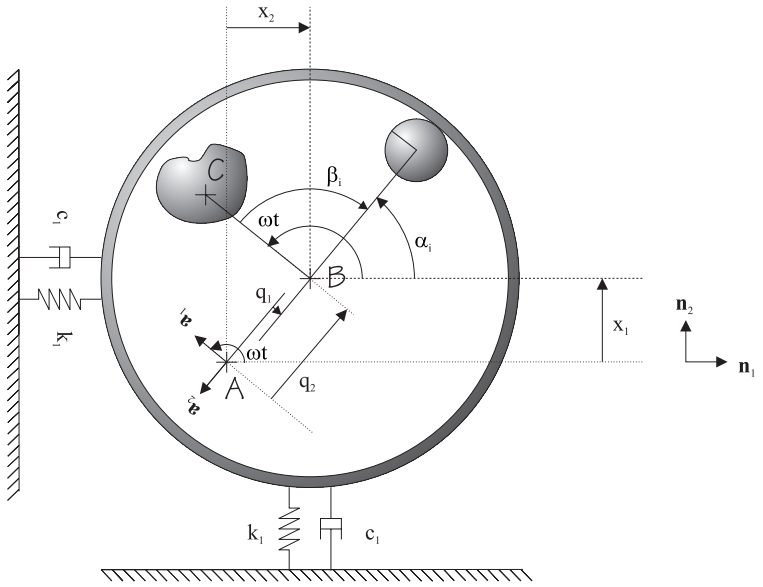

Figure 3.1: Coordinates in the rotating frame.

and

$$(m_i + \tfrac{I_i}{r_i^2}) l_i \ddot{\beta}_i + (\delta_i + \tfrac{\gamma_i}{r_i^2}) l_i \dot{\beta}_i =$$

$$m_i \left((\ddot{q}_1 - \omega^2 q_1 - 2\omega \dot{q}_2) \sin(\beta_i) + (-\ddot{q}_2 + \omega^2 q_2 - 2\omega \dot{q}_1) \cos(\beta_i) \right) \tag{3.5}$$

$$i = 1, \ldots, n.$$

We will first study a system with two correction masses. Using more than two correction masses will result in a system with a family of indifferent equilibrium positions. See chapter 5 for an explanation.

We will always assume that the correction masses have equal mass and equal distance from the axis of rotation, this will be the case in an auto-balancer with two ball bearings in a circular race filled with some viscous media. We will also assume that the parameters, δ_i, γ_i, regarding the viscous damping acting on the correction masses are equal.

3.2 Equilibrium positions

To find the equilibrium positions we first rewrite the system of equations in 3.5 and set all time derivatives to zero, the resulting equations are

$$\begin{aligned} -q_1 \sin(\beta_1) + q_2 \cos(\beta_1) = 0 \quad , \\ -q_1 \sin(\beta_2) + q_2 \cos(\beta_2) = 0 \quad . \end{aligned} \tag{3.6}$$

This can be split into two kinds of solutions. The first is when $q_{1,2}$ equals zero and $\beta_{1,2}$ are given by the system of equations in 3.4 and can be expressed as

$$\beta_1 = \pi - \cos^{-1}(\tfrac{me}{2m_1 l_1}), \tag{3.7}$$

$$\beta_2 = \pi + \cos^{-1}(\tfrac{me}{2m_1 l_1}) \quad . \tag{3.8}$$

This is the preferred solution where the system is balanced and no vibrations exists. This is actually two solutions since β_1 and β_2 can be interchanged to produce a new solution. These solutions only exist when

$$|me| \leq 2m_1 l_1. \tag{3.9}$$

The absolute value should be interpreted that e, the distance from the geometrical centre to the mass centre of the unbalanced component, can be both positive and negative. Negative e only means that the unbalance is situated at the opposite side of the defined positive side in figure 2.1. To obtain the other solutions we rewrite the equations in 3.6 as

$$\tfrac{q_2}{q_1} = \tan(\beta_1) \quad , \tag{3.10}$$

$$\tfrac{q_2}{q_1} = \tan(\beta_2) \quad . \tag{3.11}$$

This show that if $q_{1,2}$ is not equal to zero the solution in terms of $\beta_{1,2}$ can be written as

$$\beta_2 = \beta_1 + n\pi, n = 0, 1, ... \tag{3.12}$$

For $n = 0$, which means that the two correction masses are in the same place, the solution for $q_{1,2}$ in term of β_1 will be

$$q_1 = \frac{(k - \omega^2 M')(me\omega^2 + 2m_1 l_1 \omega^2 \cos(\beta_1)) + 2c\omega m_1 l_1 \omega^2 \sin(\beta_1)}{(k - \omega^2 M')^2 + (c\omega)^2} \tag{3.13}$$

$$q_2 = \frac{2(k - \omega^2 M')m_1 l_1 \omega^2 \sin(\beta_1) - c\omega(me\omega^2 + 2m_1 l_1 \omega^2 \cos(\beta_1))}{(k - \omega^2 M')^2 + (c\omega)^2} \tag{3.14}$$

Inserting 3.13 and 3.14 into 3.10 will result, after some manipulation in

$$(k - \omega^2 M')me \sin(\beta_1) + c\omega me \cos(\beta_1) + 2c\omega m_1 l_1 = 0 \tag{3.15}$$

which has a real solution if

$$(k - \omega^2 M')^2 + (c\omega)^2 \geq (c\omega)^2 \left(\frac{2m_1 l_1}{me}\right)^2. \tag{3.16}$$

Fixing all parameters except for ω, which we will vary, and letting $me < 2m_1 l_1$ we see that equation 3.16 will not have any solution for ω about $\sqrt{k/M'}$. The exact bifurcation points can be obtained by solving for the equality in equation 3.16. Also note that fixing all parameters, except for me, equation 3.16 won't have any solutions when me is below some value. The solution of 3.15 can be found in Appendix A. Equation 3.15 will, in general, have two solutions in β

Now turning back to equation 3.12 and setting $n = 1$, which physically means that the correction masses are on opposite sides, and following the same route as before results in

$$q_1 = \frac{(k - \omega^2 M')me\omega^2}{(k - \omega^2 M')^2 + (c\omega)^2}, \tag{3.17}$$

$$q_2 = \frac{-c\omega me\omega^2}{(k - \omega^2 M')^2 + (c\omega)^2}. \tag{3.18}$$

The solution for β_1 will then be

$$\beta_1 = \tan^{-1}\left(\frac{-c\omega}{k - \omega^2 M'}\right). \tag{3.19}$$

It is worth noting that equation 3.17 and 3.18 will be the equilibrium solution to a simple rotating unbalance isotropically suspended and that equation 3.19 will be the phase angle as it is usually defined. This is also two solutions since β_1 and β_2 can be interchanged to produce a new solution.

In all the system have six equilibrium positions in this coordinate representation, four of which are physically distinguishable. These four equilibrium positions are schematically drawn in figure 3.2 below.

3.3 Linear stability analysis

It is now possible to linearize equation 3.4 and 3.5 to study the stability of the four equilibrium positions. The equations of motions are put on the standard form

$$M(x)\dot{x} = f(x). \tag{3.20}$$

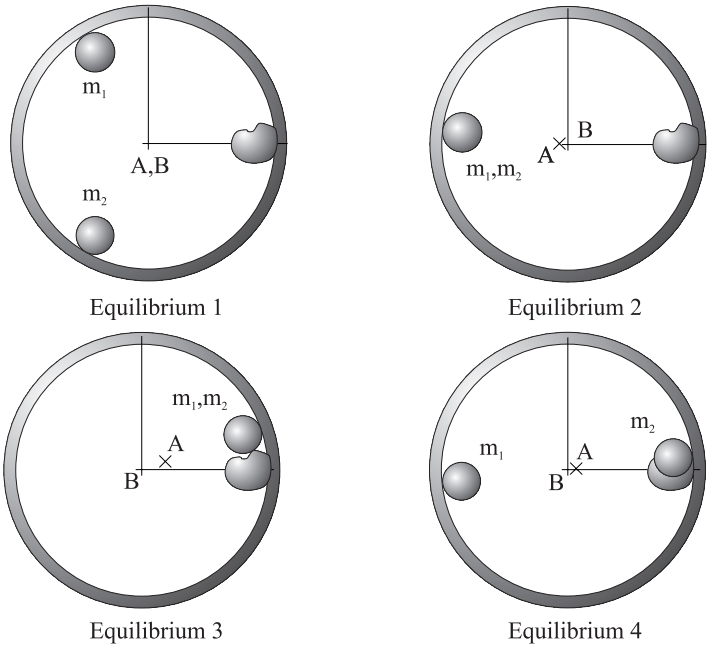

Figure 3.2: Schematically showing the 4 physical solutions. A is the centre of rotation. B is the geometrical centre. This figure is made for a particular choice of parameters. Note that all positions depend on the amount of unbalance load.

where $x = [q_1, q_2, \beta_1, \beta_2, \dot{q}_1, \dot{q}_2, \dot{\beta}_1, \dot{\beta}_2]^T$, $M(x)$ and $f(x)$ are easily derived from 3.4 and 3.5. We will now study the eigenvalues and eigenvectors for A that control the stability about the equilibrium positions where

$$A = M^{-1}(x_{0,i}) \frac{\partial f(x_{0,i})}{\partial x} \tag{3.21}$$

where $x_{0,i}$ are the four equilibrium positions. A will now be a function of the system parameters. It is possible to derive A analytically and in this case it is done with the help of Maple. However, it is not possible to derive the analytical expression for the eigenvalues and eigenvectors of A (eight order system). We therefore insert numerical values for the parameters and equilibrium positions and calculate the eigenvalues and eigenvectors of A numerically. The criterion for stability is that the eigenvalue of A with the maximum real part is negative. This would assure asymptotic stability when we are close to the equilibrium position. We therefore define the stability as

$$\omega^\star = \max_{i=1..2n} \text{real}\, \lambda_i \tag{3.22}$$

Par	Value	Par	Value
M	1.000	m_1	0.010
k	1.000	I_1/r_i^2	0.004
c	0.700	l_1	1.000
m	0.010	δ_1	0.005
e	1.000	γ_i	0.000

Table 3.1: Parameters used for stability analysis.

where λ_i are the eigenvalues of A. Thus, if $\omega^\star$ is negative the equilibrium position is stable and if its positive the equilibrium is unstable. Therefore plotting $\omega^\star$ as a function of the parameters we are interested in examining will show the stability of selected parameters. Since different λ_i will have maximum real part when parameters are varied, $\omega^\star$ will in genereal be a non-smooth function of the varied parameters.

3.4 Parameter study

What is usually of interest is to vary ω for a given system to see under what rotational speeds the system behaves as desired. It is also important, as we shall see, to investigate different amounts of unbalance by varying m and e, since we don't want a system where stability depends on the amount of unbalance. These three, or two since it is the product of m and e that is important, are the most critical when one wants to install a predesigned autobalancing device in a pre-existing system without modifying the suspension of the system. We first pick some parameter values and compare with a previous stability analysis. By setting M equal to one all other masses will be measured in terms of this unit mass. We also set k and l_1 to one. This means that lengths will be measure in terms of l_1 and spring constants in terms of k_1. For example the conversion factor between natural units of time and common units will be $\sqrt{Mk^{-1}}$.

In table 3.1 the rest of the parameters are found. These parameters correspond somewhat to the experimental machine used. By assigning a value to all parameters except for one parameter we can plot the eigenvalue with the maximum real part as a function of the varying parameter.

3.4.1 Stability when the rotational speed is varied

In figure 3.3 all parameters are assigned the values in table 3.1 and ω is varied between 0 and 6. The same plot is done for each equilibrium position.

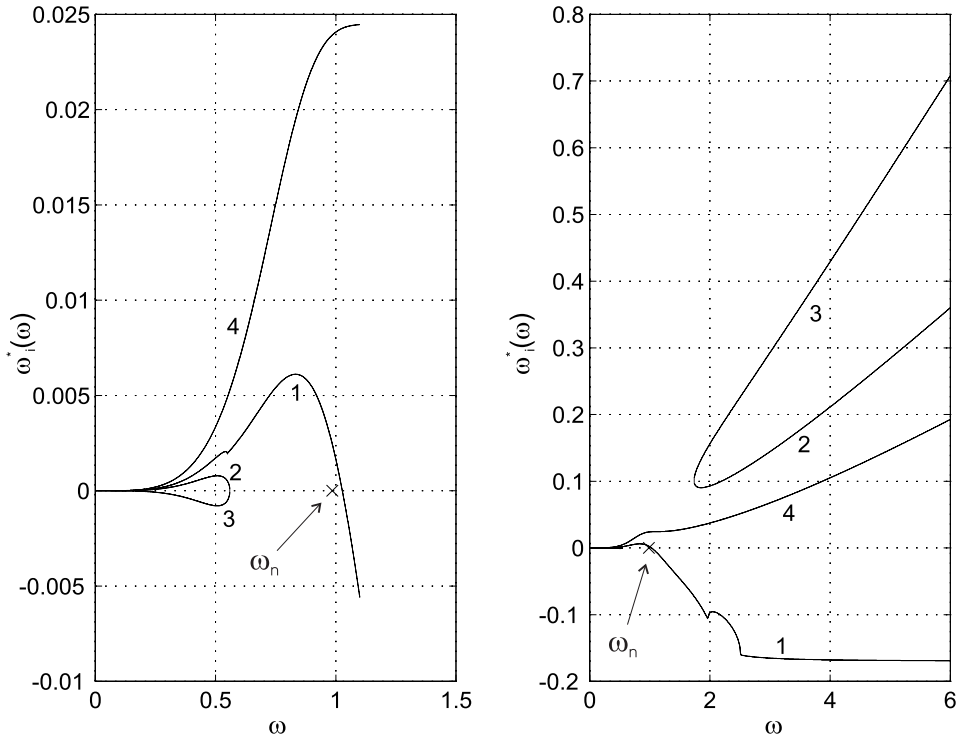

Figure 3.3: The stability as function of ω, the rotational speed. The numbers correspond to the equilibrium positions. The cross indicates the natural frequency as defined in expression 1.1. Parameters from table 3.1.

The left graph in figure 3.3 shows, for low values of ω, that we have a stable solution for type 3 equilibrium position and the rest of the equilibrium points are unstable. The third equilibrium represents a solution where the correction masses are at the same position and at the same position as the unbalance. This shows that at *low rotational speeds the correction masses will increase the unbalance* compared to a system without autobalancing.

The cross indicates the natural frequency of the system as expressed in 1.1. According to previous stability analysis made by V.I. Kravchenko *et al.*, see [2] [4] [3] the region to the left of the cross is stable. In this graph the difference between our stability point, the crossing of zero, and the point obtained in previous work is small. We will however see a greater difference when other parameters are varied. The right picture shows that at higher ω the only stable equilibrium is type 1, which is the desired equilibrium position, for the selected parameters. One of the assumptions in earlier stability analysis is that external damping is small, which corresponds to

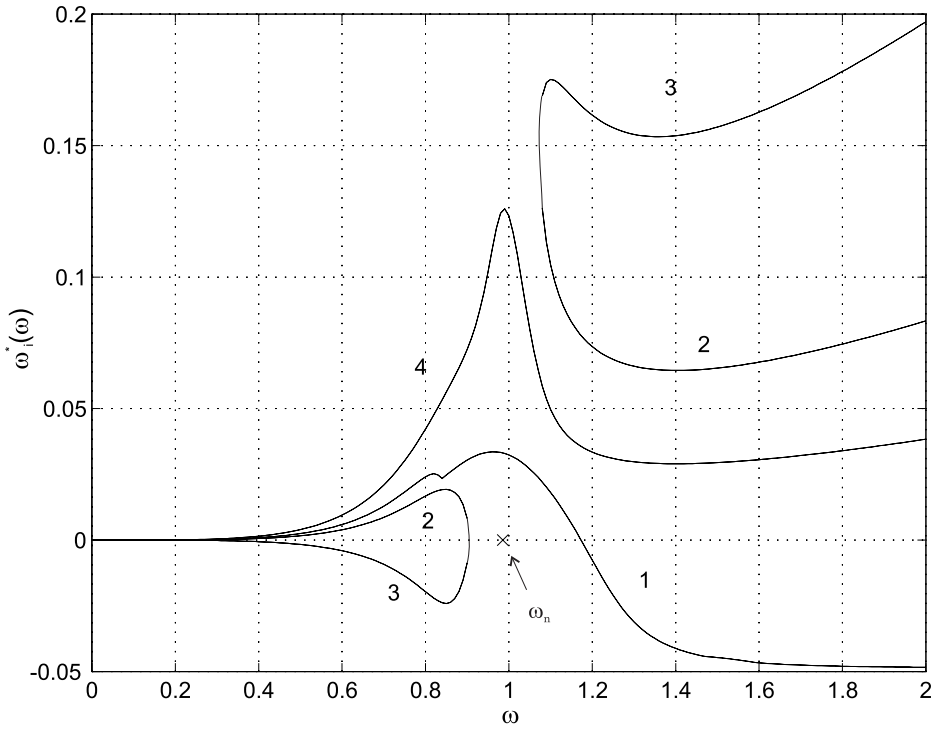

Figure 3.4: The result of decreasing c from 0.7 to 0.1 with the rest of the parameters from table 3.1.

small c here. Therefore, decreasing c should make the point where stability is attained come closer to the cross. In figure 3.4 the viscous damping c is reduced to 0.1. The result is the opposite of previous analysis. It is possible, by also decreasing the damping on the correction masses, parameter δ_1, to move the crossing point even further away from the natural frequency of the system. It is appearant that previous stability analysis oversimplified the problem.

3.4.2 Stability when the imbalance load is varied

Assume that we have a machine with parameters according to table 3.1 and running it at $\omega = 5.0$ as figure 3.3 tells us that this is a stable choice for ω and for the chosen m. It is now important to check stability when we vary the imbalance load. We vary the load by changing me in the range from zero load to 20 percent above the limit given by inequality 3.9. It is important to see what happens when the load is above the limit given by 3.9 since the

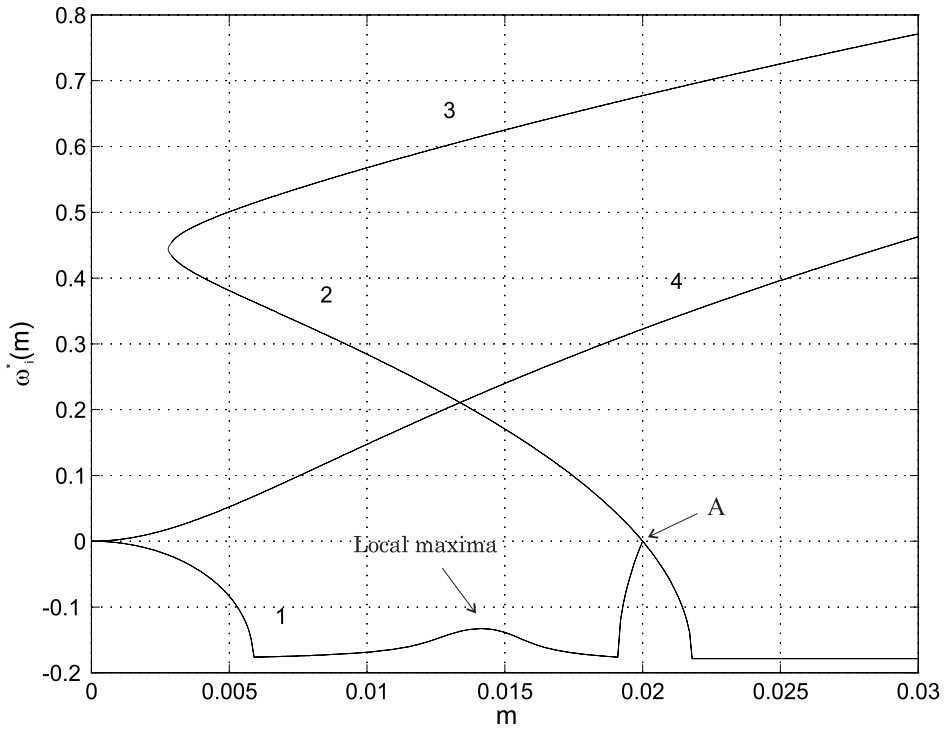

Figure 3.5: The result of varying the load by changing m. The numbers corresponds to the equilibrium positions. The angular velocity $\omega = 5$. The rest of the parameters from table 3.1.

wanted equilibrium position type 1 does not exist in this region. In figure 3.5 the result is displayed. At zero load we have an indifferent equilibrium since all positions where the compensating masses are at opposite sides are allowed. Note that equilibrium type 1 and 4 are both indifferent since they represent the same equilibrium position at zero load.

Close to maximum load, me is somewhat less than 0.002, the stability of equilibrium type 1 is lowered, point A in figure 3.5. At maximum load the stability of equilibrium type 1 and 2 coincide. When the load is above the maximum load capacity only equilibrium type 2 is stable. Only looking at equilibrium type 1 and 2 we have two stable and one unstable equilibrium when me is below maximum load (equilibrium type 1 is actually two equilibrium positions since β_1 and β_2 can be interchanged). When me is above 0.02 only one stable equilibrium exists (equilibrium type 2). We therefore have a supercritical pitchfork bifurcation at m equal to 0.02. *This is positive since it means that overloading the autobalancer, at high rotational speeds,*

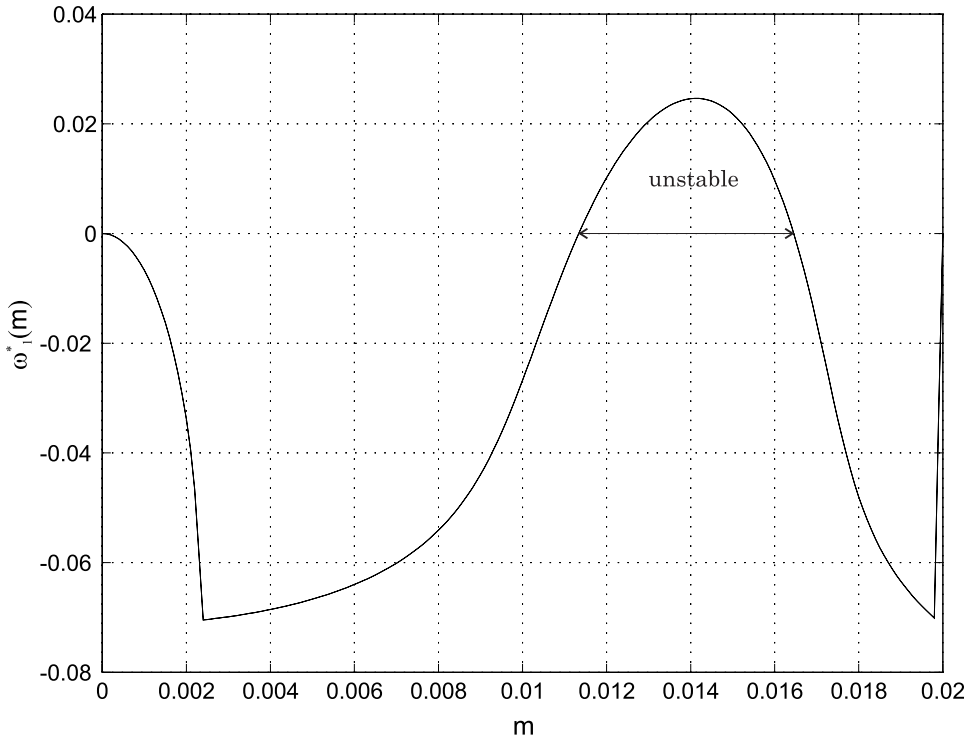

Figure 3.6: By increasing external damping and decreasing internal damping the system will be unstable for certain loads.

will result in that the two correction masses will be at opposite side of the imbalance, ie. the autobalancer will work as well as possible.

The local maxima at $me \simeq 0.014$ is interesting since it is possible to let it grow by increasing the external viscous damping and decreasing internal viscous damping. This is accomplished by increasing the external damping from $c = 0.7$ to $c = 2.7$ and decreasing the internal damping from $\delta_1 = 0.005$ to $\delta_1 = 0.002$. In figure 3.6 the local maxima has grown becoming unstable, since $\omega^\star$ is greater than zero. We then have a system where the stability depends on the amount of load. This could potentially be a problem when using an autobalancer if is not tested with all admissible loads. In figure 3.6 the local maxima has grown and become unstable. Generally it seems like *increased external viscous damping requires increased internal damping.* We can test this hypothesis by doing a contour plot of $\omega^\star$ as function of external damping c and internal damping δ_1. In figure 3.7 contour plots with different loads are found, the zero contour line divides the stable region from the unstable. As seen in figure 3.7b-d the zero contour line is increasing

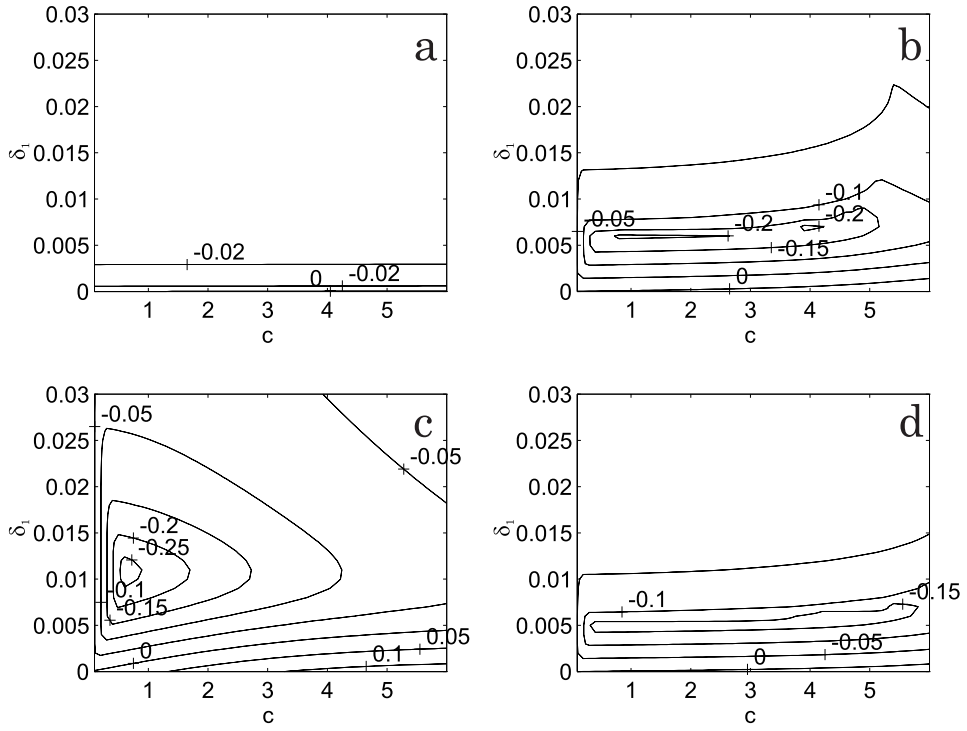

Figure 3.7: Contour plots of the maximum real part of eigenvalues as function of external damping, parameter c, and internal damping, parameter δ_1. Parameters from table 3.1 and $\omega = 5$. The load in a $m = 0.002$, in b $m = 0.008$, in c $m = 0.014$ and in d $m = 0.019$.

in internal damping with increasing external damping. It is worth noting that *optimal damping, in terms of linear stability, depends on the amount of load*. Therefore, choosing the right amount of internal damping and external damping has to be a compromise so that sufficient stability is guaranteed at all amounts of load taken from a figure such as 3.7. In figure 3.5 we see that the local maxima has a maximum at $m \simeq 0.014$. This correspond to an equilibrium position $\beta_1 \simeq \frac{3\pi}{4}$ and $\beta_2 \simeq \frac{5\pi}{4}$. From all contour plots in figure 3.8 we see that the zero contour line has a maximum in δ_1 at $m \simeq 0.014$. Therefore it seems natural to test a two correction mass autobalancer with a load so that the equilibrium positions of the two correction masses will be $\frac{3\pi}{4}$ and $\frac{5\pi}{4}$. This test would then assure stability for all other loads.

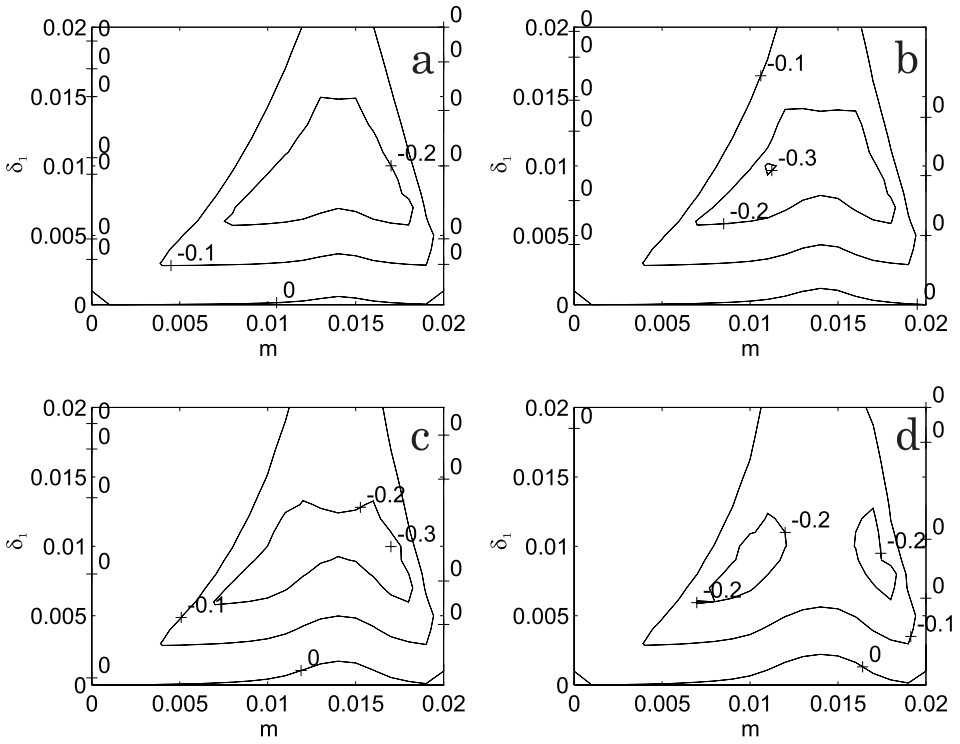

Figure 3.8: Contour plots of the maximum real part of eigenvalues as function of external load, parameter m, and internal damping, parameter δ_1. Parameters from table 3.1 and $\omega = 5$. The external damping, parameter c equals , in a 0.5, in b 1.0, in c 1.5, in d 2.0.

3.4.3 Varying the mass of the compensating masses

The maximum amount of imbalance the autobalancer can compensate for, with zero resulting amplitude, is equal to $2m_1l_1$ assuming two compensating masses of equal mass and distance from the geometric centre. Assuming that we have limited space available where the autobalancer is mounted we could increase m_1 and decrease l_1 but still keeping two times their product to a constant value given by the maximum imbalance. The dynamics of the system will then change, which can be seen by looking at equations 3.4 and 3.5. In equation 3.4 nothing will be changed since the only place where m_i and l_i occur is as a product and that is kept constant by our assumption above. However, in equation 3.5 we will have a term like $\delta_i l_i$ multiplied by $\dot{\beta}_i$ and the right hand will be multiplied by m_i. Keeping some sort of balance between the viscous forces and the right hand side forces *we expect that increasing* m_i

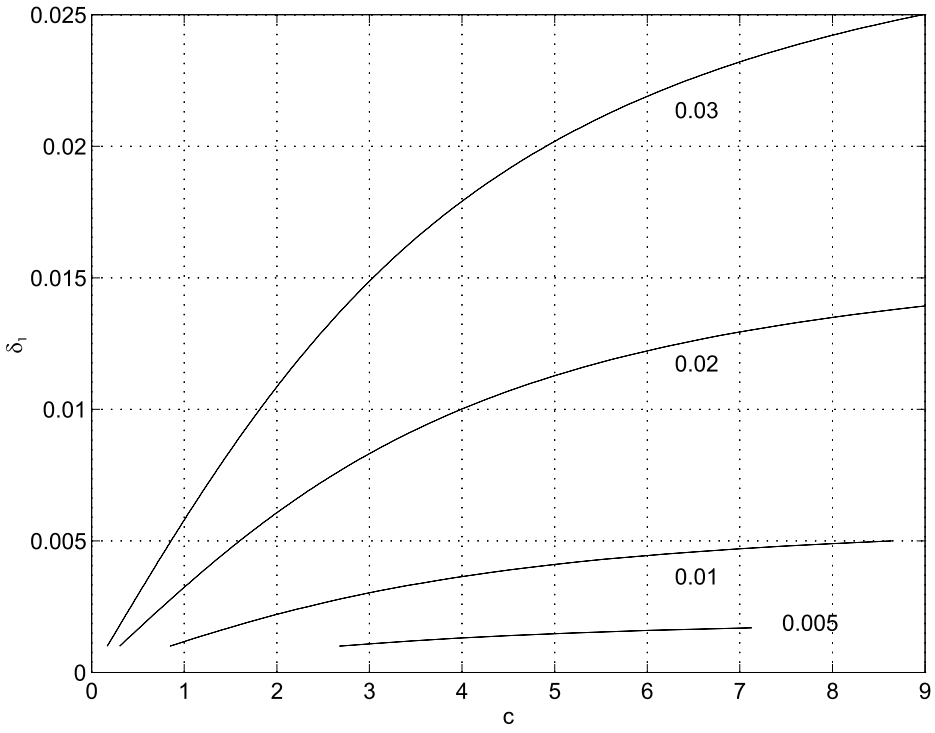

Figure 3.9: Border line dividing stable from unstable region when the mass and distance from geometrical centre to compensating masses are varied but their product is kept constant and equal to 0.01. Numbers indicating mass m_1. Regions to the northwest of border line is stable. Parameters taken from table 3.1 except for $m_1 = 0.014$

and decreasing l_i will have to be compensated for by increasing δ_i. That this is the case can be seen in figure 3.9 where the border line between stable and unstable regions have been plotted for various m_1 and l_1. cuIt also seems like the border when c is increased tends to some limiting value in δ_1. This would imply that if δ_1 *is chosen above this limiting value stability will not depend on c.* One could argue whether this low internal damping actually will occur in a real system. There are a lot of factors which actually could produce a system close to this boundary. For example in a washing machine with the drum mounted horizontally it is not desirable to activate the compensating masses at revolutions lower than the stable limit given by figure 3.3. To activate the compensating masses the viscous force must overcome the force from gravity so that the balls start moving with the outer rim. This might impose a constraint on the viscosity of the oil, lower viscosity will activate

the compensating masses at higher revolutions. Another important factor is temperature. In a system which is operating under different temperature conditions the viscosity of oil might change dramatically, maybe so much that the stability boundary is crossed.

It is also interesting to see how the stability changes when this product, $2m_1l_1$, is held constant and the mass and length is varied. In figure 3.10 two cases are compared. Line one correspond to a system where the compensating mass is equal to 0.01. Line two correspond to a mass equal to 0.05. In both systems the product $2m_1l_1$ is held constant and is equal to 0.01. The parameter controlling the viscous damping, δ_1, is increased in the second system following the reasoning above. As seen in the figure 3.10 the increased mass system shows a superior stability over the lower mass system. Also note that the first curve segment in the system with a heavier compensating mass decreases earlier and more rapidly than the low mass system. One would then expect that the system with a heavier compensating mass would perform better compared to a system with a lighter compensating mass. In section 3.6 it is shown that this the case.

3.5 Hopf bifurcations and chaos

In figure 3.9 the border line between stable and unstable regions are drawn for some different choices of system parameters. As argued before there might be situations when the internal damping is low, even so low that the border line might be crossed. It is therefore important to know what will happen when crossing the stability boundary.

A bifurcation will occur when a equilibrium point changes stability. For an excellent introduction to bifurcation theory nonlinear dynamics see [6].

If two complex conjugate eigenvalues crosses from the left half plane into the right half plane a Hopf bifurcation typically occurs. Since the real part is positive in the right half plane the equilibrium point looses its stability. When crossing the imaginary axis in this way two things can happen. We might see oscillations in the system approching some limiting amplitude resulting in a limit cycle. This is called a *supercritical* Hopf bifurcation. When the real part is small and positive the limit cycle will be sinusoidal with an angular frequency equal to the imaginary part of the crossing eigenvalues. We might also find sinusoidal oscilliations that continues to grow exponentially away from the equlibrium point. In this case local analysis can not tell what will happen. This is called a subcritical Hopf bifurcation. In engineering this is potentially a much more dangerous bifurcation, since the supercritical bifurcation will have an amplitude proportinal to $\sqrt{\mu - \mu_c}$, where μ is the

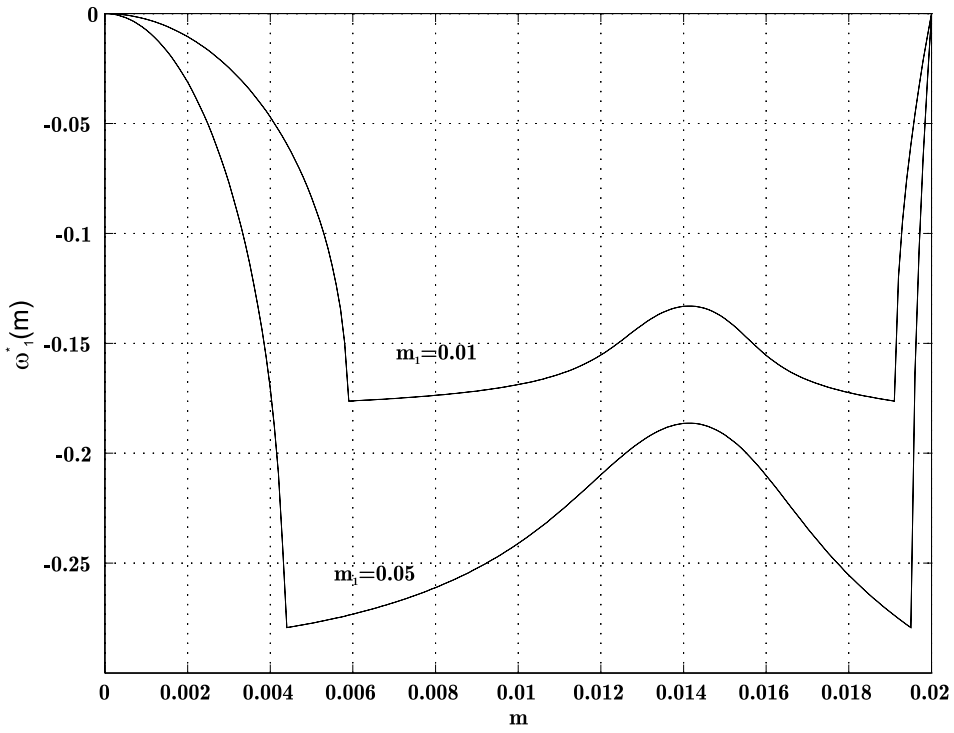

Figure 3.10: Comparison of stability when the compensating mass is increased. Line 1 $m_1 = 0.01$,$l_1 = 1$ and $\delta_1 = 0.005$. Line 2 $m_1 = 0.05$,$l_1 = 0.2$ and $\delta_1 = 0.04$. Rest of the parameters from table 3.1.

bifurcation parameter we are interested in varying and $\mu = \mu_c$ when crossing the imaginary axis. This applies for small μ's. Since our system have four degrees of freedom, which results in eight state variables, there is somewhat more to it. The dynamics of the system will approach a 2-dimensional surface embedded in the eight dimensional state space of our system. This surface is called the centre manifold. The trajectories approach this centre manifold because the other eigenvalues still have a negative real part. The shape of the surface and the dynamics on this surface depends on the parameters of the system.

If the stability boundary is crossed and a subcritical Hopf bifurcation occur, the system might experience violent vibrations due to the compensating masses movement. However, if there instead will be a supercritical Hopf bifurcation, the result will be a stable limit cycle. This stable limit cycle will manifest itself as small oscillation of the balls about their equilibrium position with resulting small vibrations of the suspended mass.

To examine this a numerical experiment can be made in the stable and the unstable regions. From figure 3.9 we have that at $\delta_1 = 0.0065$ the system will be in the stable region and that $\delta_1 = 0.0045$ it will be in the unstable region for $m = 0.02$. In figure 3.11 the phase portrait of $\beta_{1,2}$ is plotted for various values of δ_1. All trajectories are plotted after the initial transients has dissapeared. Since $\beta_{1,2}$ can be interchanged to produce a new solution, both solutions are plotted. At $\delta_1 = 0.0065$ the system remains at the stable fixpoint. At $\delta_1 = 0.0045$ a 1 periodic limit cycle exists. *This limit cycle can be observed in the experimental machine* when external damping is high or interal damping is low. There is one noticable feature of this limit cycle, one of the compensating masses has a larger amplitude than the other. This is also observed in the experimental machine. The time of the oscillations also agrees with the measured. Continuing to lower the internal damping results in period doubling. At $\delta_1 = 0.0032$ we have a 2 periodic limit cycle and at $\delta_1 = 0.00305$ we have a 4 periodic limit cycle. This results at even lower internal damping in a chaotic motion of the compensating masses. When $\delta_1 = 0.00302$ we have a chaotic motion of the system. At $\delta_1 = 0.003$ something interesting happens, the two correction masses start changing positions with each other. This would of course be hard to realize since that would mean that the balls would have to move through each other. That some sort of Hopf bifurcation occur can be seen in figure 3.12 where one pair of eigenvalues are crossing the real axis when the internal damping δ_1 is varied from 0.01 to 0.003.

Using centre manifold theory and normal form analysis it is possible to calculate whether a stable or unstable Hopf bifurcation will occur. This was done for the border in figure 3.9 where $m = 0.02$. These calculations show that a stable Hopf bifurcation will occur for this particular border. This in combination with the experimental machine would indicate that a *stable Hopf bifurcation will occur when the internal damping acting on the compensating masses are lowered.*

3.6 Numerical experiments

We have employed a local stability analysis, i.e. we examined the stability of the linearized equations of motion about the equilibrium position. It is therefore interesting to examine whether local stability will influence the complete motion. To see this we could devise some rules which determines a good performance from a poor one and run a series of time simulations. These simulations can then be compared to the local stability analysis. As usual the problem is to decide what separates a good performance from

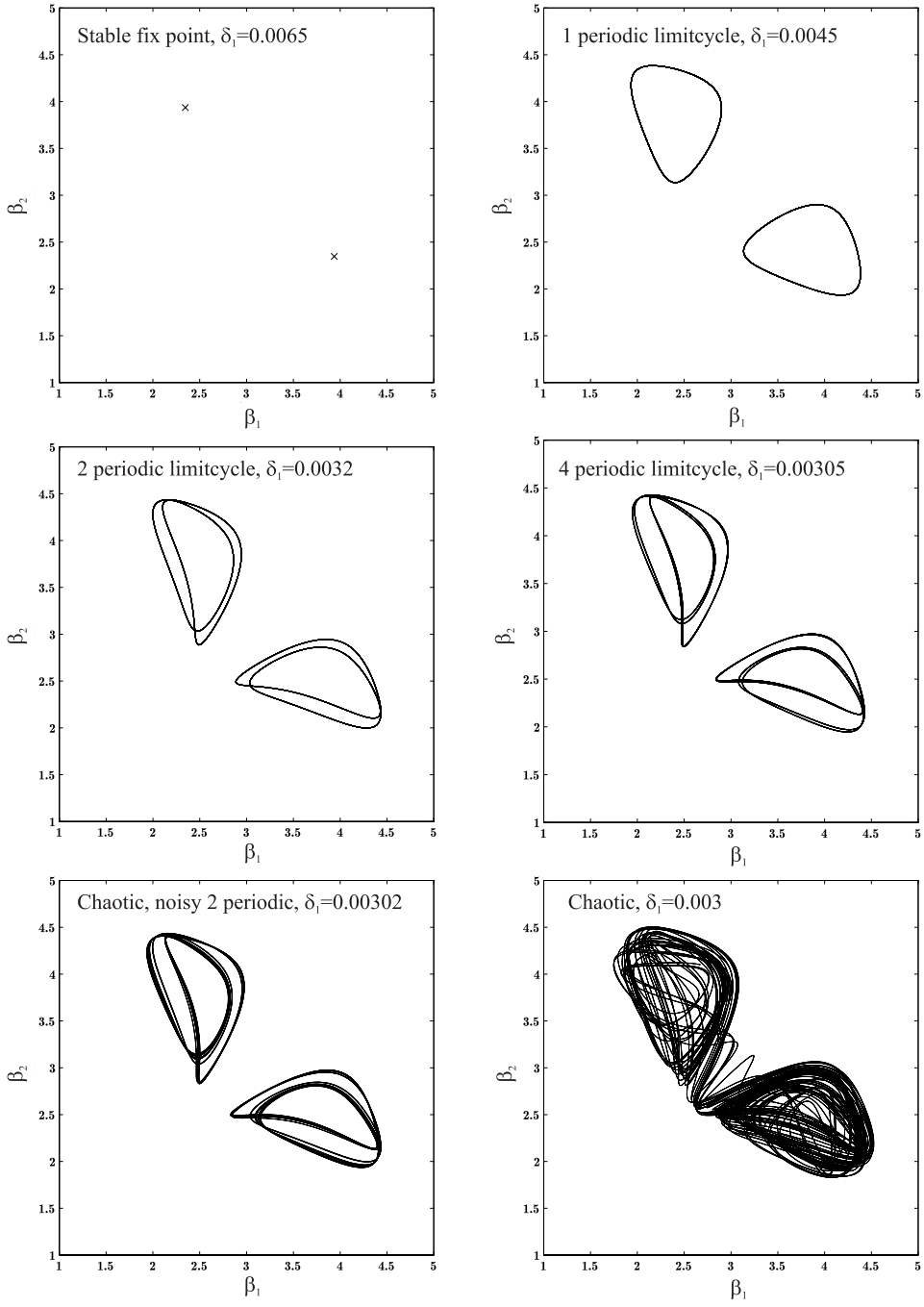

Figure 3.11: Phase portrait of $\beta_{1,2}$ when varying the internal damping δ_1. Period doubling occurs and at low internal damping chaotic motion is found.

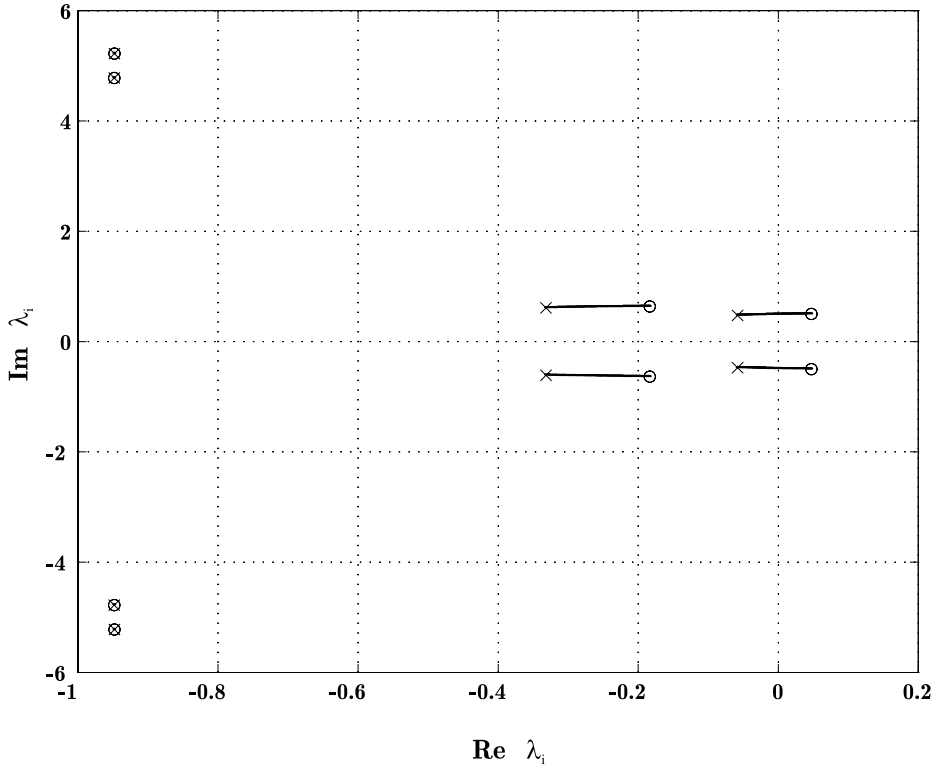

Figure 3.12: Showing the crossing of eigenvalues of the real axis when δ_1 is varied. Cross indicates $\delta_1 = 0.01$ and ring $\delta_1 = 0.003$.

a poor one. To the authors knowledge there does not exist any accepted performance test to evaluate autobalancers. The following is proposed as a candidate for such criteria. In most cases an autobalancer is fitted where one can not foresee the amount of unbalance and its position. Therefore the most common situation will be that the autobalancer is compensating for an unbalance and suddenly this amount of unbalance and its position change. A corresponding time simulation will then have initial conditions; all speeds are set to zero and the position of the axis of rotation is at the geometrical centre. The angular position of the correction masses are chosen randomly which corresponds to a system balancing some unbalance at some position. The new unbalance situated at zero angular position is randomly chosen and within the maximum balancing capability. We could then measure the time or number of revolutions until the amplitude of the oscillations are below some specified value. This value could be a fraction of the maximum amplitude in the simulation or some value determined by what is acceptable

Par	Value(Common)
M	1.000
k	1.000
m	0 - 0.02
e	1.000
γ_i	0.000

Par	1	2	3
c	1.8	0.7	0.7
δ_1	0.003	0.005	0.003
m_1	0.01	0.01	0,05
l_1	1.0	1.0	0.2
I_1/r_i^2	0.004	0.004	0.040

Table 3.2: Parameters used for numerical comparison.

as amplitude. To test this evaluation method 10000 numerical simulations were made on some different choices of parameters. The measurement used were the number of revolutions before the amplitude becomes permanently smaller than one fifth of $2m_1l_1/M$. The amplitude $2m_1l_1/M$ correspond to the amplitude one would have if the unbalance me equals $2m_1l_1$ and the rotary speed ω is much greater than the natural frequency of the system. In figure 3.13 the stability of three different parameter choices is plotted , when the load is varied. The parameters used can be found in table 3.2. In the left table the parameters that are common to all three system are found. In figure 3.14 the outcome is displayed as a histogram over the number of revolutions. The mean value and standard deviation is also displayed. The first system has relatively high external damping c_1 and low internal damping δ_1 compared to system two. System one has somewhat better stability at low loads but worse at the middle region compared to system two. System one and two have identical compensating masses. System two clearly behaves better than system one, both the mean value and the standard deviation is lower than in system one. Since figure 3.13 only displays the stability of the linearized system there is no reason to expect that the full nonlinear system will behave the same way. We are not even guaranteed that the system will tend to the equilibrium position. However these three histogram display the result of 30000 simulations and not one has not reached the equilibrium position. The idea is that when the system is reaching its equilibrium position it has to spend some time in the region where the linear model accurately models the behavior and therefore it should have some correspondence with the outcome in the histograms. In system three the mass of the compensating mass is increased five times over system one and two. The length l_1 is also reduced to one fifth of system one and two. Following the reasoning in section 3.4.3 the internal damping δ_1 is increased to compensate for the inertial forces due to a heavier mass. As seen in figure 3.13 this system show a higher stability than both system one and two. The outcome of the numerical simulations is displayed in histogram three of figure 3.14. Parameter set three shows both

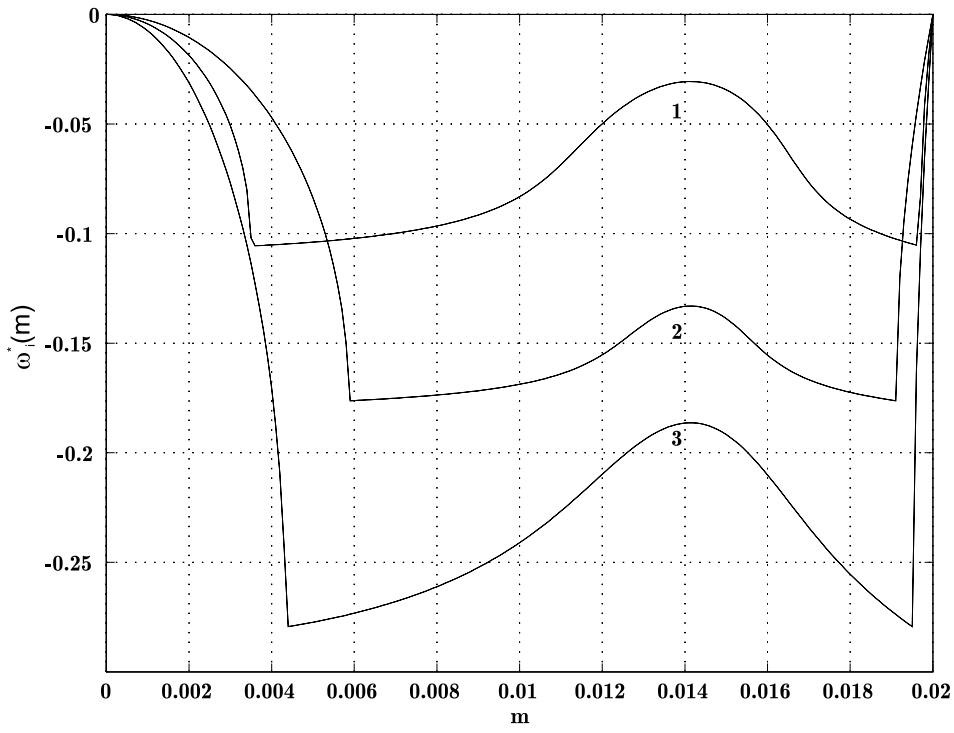

Figure 3.13: Stability when the load is varied. The three different plots correspond to the parameters found in table 3.1.

lower mean value and lower standard deviation than both system one and two. It therefore seems that one should *choose heavier compensating masses close to the axis of rotation over lighter masses far from the axis of rotation*. It also seems that the local stability tells something about the dynamics of the global system and can be used as a reasonable guide to optimize a system.

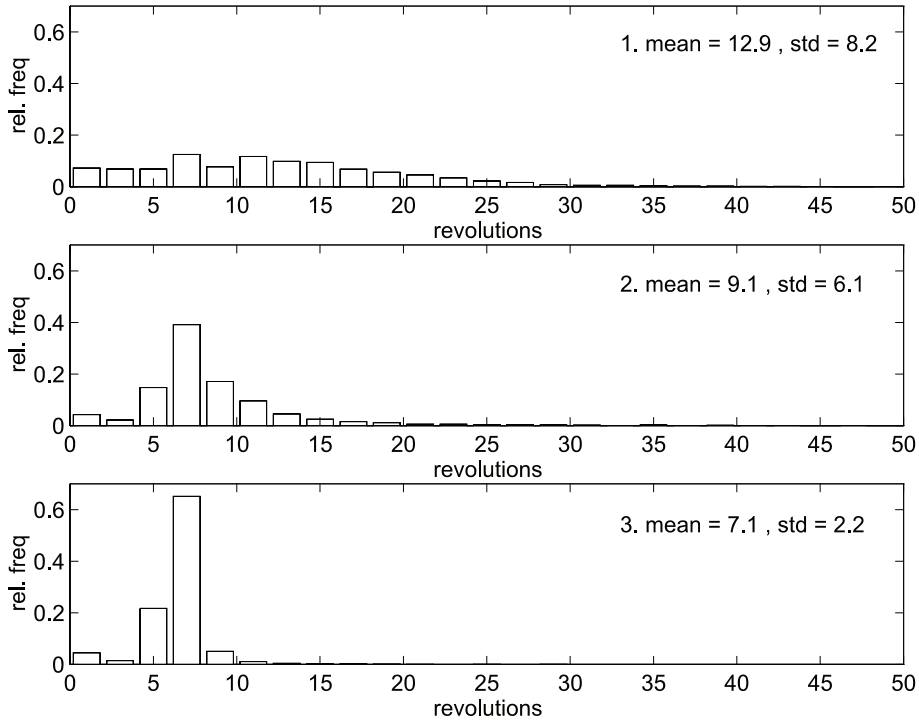

Figure 3.14: The relative frequency of number of turns before the amplitude is below one fifth of the maximum amplitude due to a simple rotating unbalance.

Chapter 4

Anisotropic case

4.1 Derivation of equations

Most constructions where an autobalancer might fit in is clearly anisotropic. For example a common use of autobalancers are in washing machines. When spin drying the wash is not evenly distributed and as result of this an unbalance exist. The suspension in washing machines is not isotropic since the drum is usually standing on or hanging from springs almost vertically mounted. This will give a much lower natural frequency in the horizontal plane than in the vertical plane. It should be noted that using autobalancing techniques in washing machines requires two balancing rings, since the location along the axis of rotation of the unbalance is not static. Also there might exist dynamic unbalance in a washing machine. Using two balance rings solves both these problems. Another anisotropic case occurs when a grinding machine is operated. When a grinding machine is operated the suspension parameters will depend on the configuration and whether the grinder is in contact with the work piece or not.

The equations used in the anisotropic analysis are equations 2.1, 2.2 and 2.3 with the substitution 3.3. Using substitutions 3.1 and 3.2 will result in lengthy equations which are more time consuming to compute numerically than equations 2.1, 2.2 and 2.3 with the substitution 3.3. Substitution 3.3 is used so that the state, when the system is balanced, will be at zero speed in all state variables. Using substitution 3.3 the equations of motion will look like

$$M'\ddot{x}_1+c_1\dot{x}_1+k_1x_1 = me\omega^2\cos(\omega t)+\sum_{i=1}^{i=n} m_i l_i(\ddot{\beta}_i\sin(\beta_i+\omega t)+(\dot{\beta}_i+\omega)^2\cos(\beta_i+\omega t)), \tag{4.1}$$

$$M'\ddot{x}_2+c_2\dot{x}_2+k_2x_2 = me\omega^2\sin(\omega t)+\sum_{i=1}^{i=n} m_i l_i(\ddot{\beta}_i\cos(\beta_i+\omega t)-(\dot{\beta}_i+\omega)^2\sin(\beta_i+\omega t)), \tag{4.2}$$

$$\begin{aligned}(m_i+\tfrac{I_i}{r_i^2})l_i\ddot{\beta}_i + l_i(\delta_i+\tfrac{\gamma_i}{r_i^2})\dot{\beta}_i = \;& m_i(\ddot{x}_1\sin(\beta_i+\omega t)-\ddot{x}_2\cos(\beta_i+\omega t)) \\ & i=1,\ldots,n \end{aligned} \tag{4.3}$$

where M' equals $(M+m+\sum_{i=1}^{n} m_i)$, as before, and is introduced since it occurs frequently. We we still use the assumption that the parameters describing the compensating masses are equal and that the balancing device is capable of balancing the unbalance, i.e.

$$me \leq 2m_1l_1. \tag{4.4}$$

The only equilibrium position in this coordinate representation will be

$$q_1 = 0, \tag{4.5}$$
$$q_2 = 0, \tag{4.6}$$
$$\beta_1 = \pi - \cos^{-1}(\tfrac{me}{2m_1l_1}) \quad , \tag{4.7}$$
$$\beta_2 = \pi + \cos^{-1}(\tfrac{me}{2m_1l_1}) \quad . \tag{4.8}$$

4.2 Linear stability analysis

We now have an explicit time dependence in the equations of motion. The way to go for calculating the stability of the equilibrium position is to use Poincaré maps. The equations of motions can be written as

$$M(x,t)\dot{x} = f(x,t) \tag{4.9}$$

where $x = [x_1, x_2, \beta_1, \beta_2, \dot{x}_1, \dot{x}_2, \dot{\beta}_1, \dot{\beta}_2]^T$. Both $M(t,x)$ and $f(x,t)$ are $\frac{2\pi}{\omega}$ periodic, as can be seen from equations 4.1 to 4.3. It therefore seems natural to look at the configuration at intervals of $\frac{2\pi}{\omega}$ in t. The k'th intersection of the Poincaré map will then be when $t = \frac{2\pi}{\omega}k$. The Poincaré map is then defined by

$$x_{k+1} = \Phi(x_k, 2\pi/\omega) \tag{4.10}$$

where $\Phi(x,t)$ is the flow of solutions i.e. $\Phi(x,t)$ represents all solutions to 4.9 with initial conditions $\Phi(x,0) = x$. If we have a equilibrium x_0, clearly $x_0 = \Phi(x_0, 2\pi/\omega)$. In the general case x may vary with time between the intersections. However, in our case the equilibrium is given by 4.5 to 4.8

and does not vary in time. Wheter this equilibrium is stable or not depends on the derivatives of $\Phi(x_0, 2\pi/\omega)$ with respect to x. The criterion for a equilibrium position to be stable is that the eigenvalues of $\Phi_x(x_0, 2\pi/\omega)$ have a magnitude that is less than one. To calculate $\Phi_x(x_0, 2\pi/\omega)$ we start with inserting $\Phi(x, t)$ into 4.9, this gives

$$M(\Phi, t)\Phi_t = f(\Phi, t). \tag{4.11}$$

We then take the implicit derivative with respect to x, which result in,

$$M_x(\Phi, t)\Phi_x\Phi_t + M(\Phi, t)\Phi_{t,x} = f_x(\Phi, t)\Phi_x \tag{4.12}$$

In our case $\Phi(x_0, t) = x_0$, thus it does not depend on t and its derivative with respect to t is therefore zero. We are then left with

$$M(x_0, t)\Phi_{t,x} = f_x(x_0, t)\Phi_x. \tag{4.13}$$

Changing the order of differentiation of $\Phi_{t,x}$ and inverting M gives

$$\Phi_{x,t} = M^{-1}(x_0, t)f_x(x_0, t)\Phi_x. \tag{4.14}$$

which is a differential equation for Φ_x. The initial condition for Φ_x comes from differentiating $\Phi(x, 0) = x$ with respect to x, i.e. $\Phi_x(x, 0) = I$ where I is the identity matrix. This differential equation is, in our case, numerically integrated to produce $\Phi_x(x_0, 2\pi/\omega)$.

By looking more carefully at equations 4.1 to 4.2 we see that there exists a symmetry under the simple substitution

$$t \rightarrow t + \frac{\pi}{\omega}, \tag{4.15}$$

$$x_{1,2} \rightarrow -x_{1,2}, \tag{4.16}$$

$$\beta_{1,2} \rightarrow \beta_{1,2} \tag{4.17}$$

which will give equations 4.1 to 4.2 again. Therefore, we only have to integrate 4.14 over the interval $t : \epsilon : [0, \pi/\omega]$ and using the symmetry to calculate $\Phi_x(x_0, 2\pi/\omega)$. The symmetry can be written as

$$\Phi_x(x_0, 2\pi/\omega) = \left[\begin{bmatrix} -1 & 0 & 0 & 0 & 0 & 0 & 0 & 0 \\ 0 & -1 & 0 & 0 & 0 & 0 & 0 & 0 \\ 0 & 0 & 1 & 0 & 0 & 0 & 0 & 0 \\ 0 & 0 & 0 & 1 & 0 & 0 & 0 & 0 \\ 0 & 0 & 0 & 0 & -1 & 0 & 0 & 0 \\ 0 & 0 & 0 & 0 & 0 & -1 & 0 & 0 \\ 0 & 0 & 0 & 0 & 0 & 0 & 1 & 0 \\ 0 & 0 & 0 & 0 & 0 & 0 & 0 & 1 \end{bmatrix} \Phi_x(x_0, \pi/\omega)\right]^2. \tag{4.18}$$

Par	Value	Par	Value
M	1.000	e	1.000
k_1	1.000	m_1	0.010
c_1	0.700	I_1/r_i^2	0.004
k_2	0.500	l_1	1.000
c_2	0.350	δ_1	0.005
m	0.010	γ_i	0.000

Table 4.1: Parameters used for the anisotropic stability analysis.

Since stability is governed by the eigenvalues of $\Phi_x(x_0, 2\pi/\omega)$ we define

$$\omega^{**} = \max_{i=1..2n} \mid \lambda_i \mid$$

where λ_i are the eigenvalues of $\Phi_x(x_0, 2\pi/\omega)$. The stability ω^{**} is then plotted as a function of the parameters we are interested in varying and when it is below one the equilibrium point is stable. The difference here compared to to the isotropic case, found in section 3.3, is that ω^{**} will now show the amplitude decay per turn compared to ω^*, in the isotropic case, which show the exponential decay in time.

4.3 Parameter study

We start our stability examination by varying ω for a system given by parameters from table 4.1 below. This particular choice of parameters will give a system where the natural frequencies will be quite close to each other and their ratio will be equal to $\sqrt{2}$. In figure 4.1 ω is varied from zero to seven. Note the similarities compared to figure 3.3. In previuos stability analysis the region between the leftmost cross and middle cross was considered stable and the region between the middle and rightmost cross unstable. To the right of the rightmost cross the region was considered stable. By separating the natural frequencies in the horizontal and vertical direction with a higher ratio than given by the parameters in table 4.1 we will get a stable middle region. In figure 4.2 the ratio of natural frequency in the horizontal and vertical direction is 10. This explains why it is possible to mount an autobalancer more stiffly in one direction compared to the other and run it at a rotary speed between the natural frequencies in horizontal and vertical direction. In this case the previous stability results predicts the middle region quite accurately but fails to predict the stability in the high ω region. In general we will have a stable middle region when we have large separation of natural frequencies

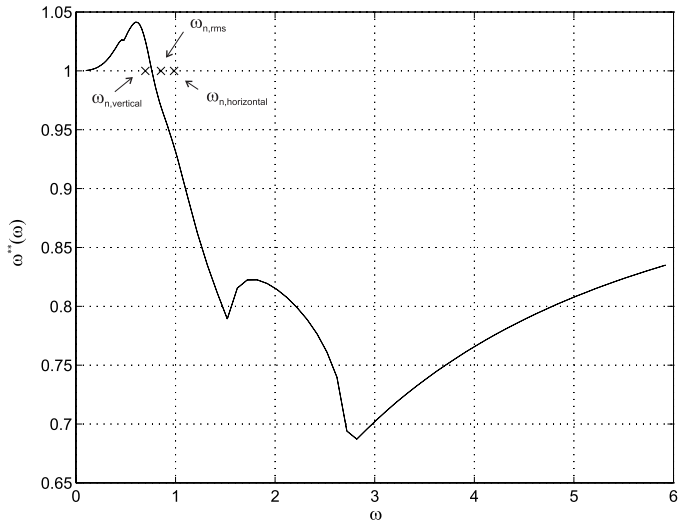

Figure 4.1: The stability as a function of the rotational speed. The crosses indicate the natural frequencies in the vertical direction and in the the horizontal direction. The middle cross indicates the rms of the two frequencies. Parameters from table 4.1.

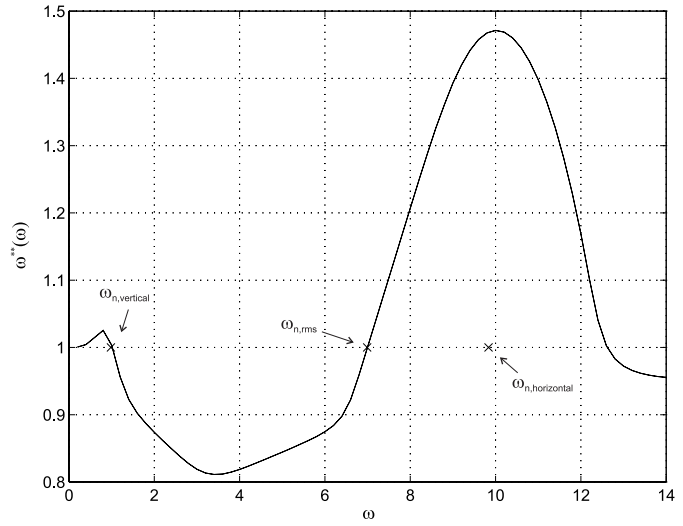

Figure 4.2: The stability as a function of ω when the spring constant in the horizontal and the vertical direction differs greatly. Parameter values from table 4.1 except for $k_2 = 100$, $c_2 = 0.7$ and $m = 0.014$.

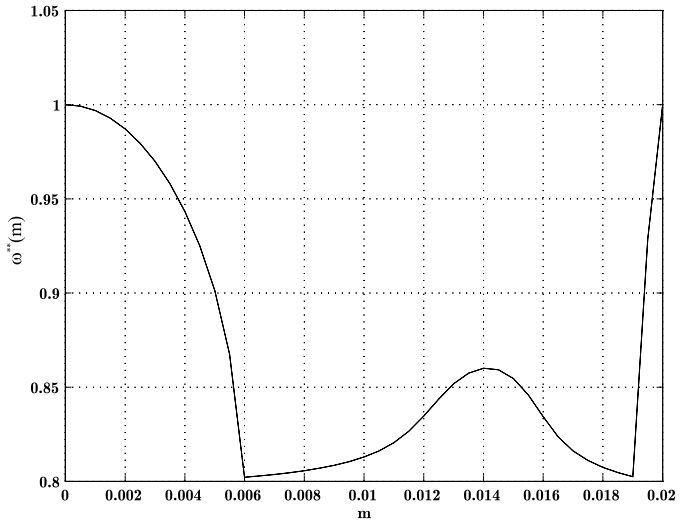

Figure 4.3: The result of varying the unbalance load by changing m. The angular velocity $\omega = 5$. The rest of the parameters from table 4.1.

and no stable middle region when we have low separation. We can also infer from figure 4.2 that we should run an autobalancer with these parameters at $\omega \simeq 3.5$ if we want maximum decay in amplitude per turn. If instead we are interested in maximum decay in time we can run the autobalancer somewhere between $\omega \simeq 3.5$ and $\omega \simeq 6.3$.

4.3.1 Stability when the imbalance load is varied

The anisotropic case with varying load show the same behaviour as the isotropic case. In figure 4.3 the load is varied in the range where the autobalancer is capable of balancing. The figure shows the same features as the figure in the isotropic case. The local maxima at $m \simeq 0.014$ is still present, corresponding to a equilibrium position of the compensating masses where $\beta_1 \approx \frac{3\pi}{4}$ and $\beta_2 \approx \frac{5\pi}{4}$. It is possible by decreasing the viscous damping acting on the compensating masses to let the local maxima grow and become unstable. It is also useful to examine the case when we are running at a rotational speed between the two natural frequencies. In figure 4.4 , $\omega = 5$, which is between the two natural frequencies. The stability plot is similar to the other stability plots when m is varied.

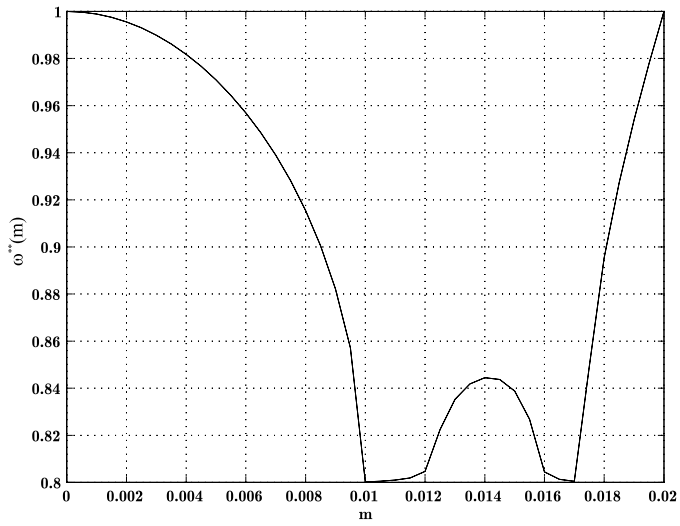

Figure 4.4: The result of varying the unbalance load by changing m when running at a revolutionary speed between the two natural frequencies. The angular velocity $\omega = 5$. Parameters from table 4.1 except $k_2 = 100$ and $c_2 = 0.7$.

Chapter 5

Multiple correction masses

5.1 Introduction

Using only two correction masses is usually not volume efficient since there will be a lot of unused space in the balance rings. This, of course, depends on the design of the balancing ring, but since most balance rings use ballbearings with a radius which is less than the radius of the balance rings, more than two balls are more volume efficient. Using more than two correction masses results in a system capable of correcting for a higher imbalance load. The maximum number of correction masses to use is the amount which fills half the ring with correction masses.

5.2 Equilibrium positions

An aspect of using more than two correction masses is that we will get a family of equilibrium positions where the compensating masses correct for the unbalance. For example when we have three correction masses we will have a one parameter family of equilibrium positions. Figure 5.1 show that there will be a combined centre of mass of the unbalance and the third correction mass. The position of the combined centre of mass is labeled D in figure 5.1. We call this the new unbalance. By varying the angular position, angle β_3, of the third correction mass, the point D will take different positions. In order to calculate the equilibrium position of the two other correction masses the distance from the geometrical centre to the centre of gravity of the new unbalance is needed. Labeling this distance, in the figure from B to D, with e' it can be expressed as

$$e' = \frac{\sqrt{(m_1 l_1 \sin\beta_3)^2 + (me + m_1 l_1 \cos\beta_3)^2}}{m + m_1}. \tag{5.1}$$

Now exchanging e for e' and m for $m+m_1$ the expressions for the equilibrium positions 3.7-3.8 are valid with the exception that an angle α is added to β_1 and β_2. This angle compensates for the new angular position of the unbalance, see figure 5.1. Note that α is the angle between BC and BD and can be expressed as

$$\alpha = \text{atan2}(m_1 l_1 \sin\beta_3, me + m_1 l_1 \cos\beta_3) \tag{5.2}$$

where atan2 is the two argument arctangent function. We can not choose any value for β_3 since the last two correction masses must be able to corrrect for the new unbalance. This can be stated as

$$(m + m_1)e' \leq 2m_1 l_1. \tag{5.3}$$

Inserting the expression for e' and equating this for β_3 gives

$$\cos\beta_3 \leq \frac{3(m_1 l_1)^2 - (me)^2}{2mem_1 l_1}. \tag{5.4}$$

This shows, as expected, that if the imbalance is less or equal to $m_1 l_1$ we can freely vary β_3. For the parameter study it is worth observing that we only need to vary β_3 in the region 0 to π since it will be symmetric to the region 0 to $-\pi$.

In the anisotropic case this equilibrium position will be the only one in this coordinate representation. However, the isotropic case will have some more equilibrium positions. To derive these equilibrium positions we return to equation 3.5. Setting all time derivatives to zero we get

$$-q_1 \sin\beta_i + q_2 \cos\beta_i = 0, i = 1, 2, 3. \tag{5.5}$$

The solutions of this, in terms of β_i are,

$$\beta_2 = \beta_1 + n\pi, : n = 0, 1, \tag{5.6}$$
$$\beta_3 = \beta_1 + k\pi, : k = 0, 1 \tag{5.7}$$

which corresponds to two physical solutions since $n = 0, k = 1$ is physically equal to $n = 1, k = 0$ and $n = 1$ and $k = 1$. The two physical solutions are that the correction masses are at the same angular positon $\beta_1 = \beta_2 = \beta_3$ and that one of the correction masses is at the opposite side $\beta_1 = \beta_2 = \beta_3 - \pi$. If we would have four correction masses we would also have the case where there are two correction masses together on opposite sides. The solutions for q_1 and q_2 can easily be obtained from the equilibrium equations given

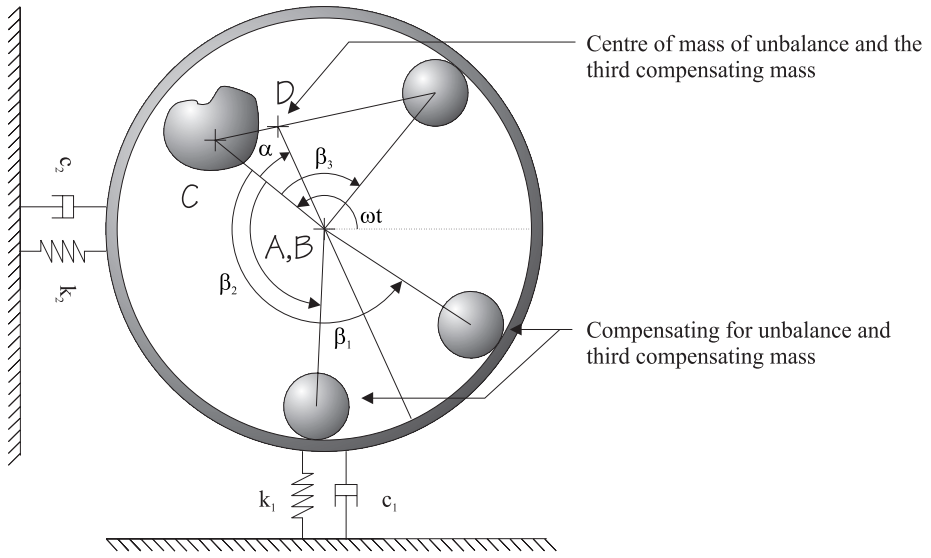

Figure 5.1: Using more than two correction masses will, depending on the unbalance load, result in a family of equilibrium positions. The equilibrium positions will therefore be indifferent.

in section 3.2. Obtaining the first solution when $\beta_1 = \beta_2 = \beta_3$ is done by replacing $2m_1$ with $3m_1$ in equations 3.13,3.14 and results in

$$q_1 = \frac{(k-\omega^2 M')(me\omega^2 + 3m_1 l_1 \omega^2 \cos\beta_1) + 3c\omega m_1 l_1 \omega^2 \sin\beta_1)}{((k-\omega^2 M')^2 + (c\omega)^2}, \quad (5.8)$$

$$q_2 = \frac{3(k-\omega^2 M')m_1 l_1 \omega^2 \sin\beta_1 - c\omega(me\omega^2 + 3m_1 l_1 \omega^2 \cos\beta_1))}{(k-\omega^2 M')^2 + (c\omega)^2}. \quad (5.9)$$

This will result in, in terms of β_1

$$(k-\omega^2 M')me\sin\beta_1 + c\omega me\cos\beta_1 + 3c\omega m_1 l_1 = 0 \quad (5.10)$$

which has a real solution if

$$(k-\omega^2 M')^2 + (c\omega)^2 \geq (c\omega)^2 \left(\frac{3m_1 l_1}{me}\right)^2. \quad (5.11)$$

This shows that depending on the choice of parameter values there might not exist a real solution. Equation 5.10 has two roots resulting in two physically different solutions. The next case, when $\beta_1 = \beta_2 = \beta_3 - \pi$, is similar to the above except that $3m_1$ has to replaced by m_1. The reason why this can be done is that the opposite side correction mass, labeled 3, will compensate for

the correction mass labeled 2 leaving only correction mass number 1. This case will also result in two physically different solutions. *All in all we have five physically distinguishable solutions.* If we were to extend to use greater number of correction masses we would have for four correction masses, six equilibrium positions and five would give seven and so on.

These solutions only exists when both q_1 and q_2 are equal to zero. This is important since one could else believe that there exist solutions when $\beta_1 = \alpha$ and $\beta_2 = \alpha + \pi$. However this is not possible since compensating mass 3, angle β_3, is not rigidly connected to the unbalance and would in this case start to move. This is the case for the other unbalanced solutions as well.

5.3 Linear stability analysis

The stability analysis is performed by linearization of the equations of motion given by equation 3.4 and 3.5. The equations of motion are put in the form

$$M(x)\dot{x} = f(x) \tag{5.12}$$

where x now equals $[q_1, q_2, \beta_1, \beta_2, \beta_3, \dot{q}_1, \dot{q}_2, \dot{\beta}_1, \dot{\beta}_2, \dot{\beta}_3]^T$. The linear stability is now governed by A, which equals

$$A(x_{0,i}) = M^{-1}(x_{0,i})\frac{\partial f(x_{0,i})}{\partial x}, : i = 1, .., 5 \tag{5.13}$$

where $x_{0,i}$ are the five equilibrium positions given in the previous section. A can be derived analytically but the eigenvalues and eigenvectors are calculated numerically. Since the first equilibrium position, where the system is balanced and no vibrations exists, is indifferent, we expect that one of the eigenvalues of $A(x_{0,1})$ should be zero. The condition for stability is that the rest of the eigenvalues are less than zero. Therefore we define the stability as

$$\omega_j^{***} = \max_{i=1..2n-1} \mathrm{Re}\,\lambda_i \tag{5.14}$$

where λ_i are the eigenvalues of $A(x_{0,j})$ and λ_{2n} is the zero eigenvalue and is therefore removed. It is important to check stability for all admissible values of β_3 since $x_{0,1}$ is a function of β_3. If the stability condition holds for all admissible values of β_3 the system will certainly selfbalance if you are close to the equilibrium position. It is also important to check the stability of the other equilibrium positions since we don't want them to be stable in the operating region.

Par	Value	Par	Value
M	1.000	e	1.000
k_1	1.000	m_1	0.010
c_1	0.700	I_1/r_i^2	0.004
k_2	0.500	l_1	1.000
c_2	0.350	δ_1	0.005
m	0 - 0.03	γ_i	0.000

Table 5.1: Parameters used for multiple mass stability analysis.

5.4 Parameter study

The parameter study is complicated by the fact that we now have to vary not only the parameter we are interested in but also the equilibrium position. Starting with the parameters found in table 5.1 where we vary the load between 0 and 0.3 which is the maximum load the system is capable of balancing. The stability ω_j^{***} is plotted as a contour plot since this controls the asymptotic behaviour of small disturbances. In figure 5.2 the greyed area in the upper left corner corresponds to the condition found in 5.4 for β_3. The zero at $m = 0.1$ and $\beta_3 = \pi$ is the result of another indifferent equilibrium position, namely that the balancing mass and correction mass are of equal mass. Since they are on opposite side the two other correction masses they may assume any position where they are on opposite side. From figure 5.3, where the stability for the five other equilibrium positions are plotted, we see that they are all unstable in the regime where the autobalancer is capable of balancing the imbalance. When overloaded the balanced equilibrium cease to exist. Equilibrium type 5 then becomes the only stable one. This equlibrium position physically corresponds to the three compensating masses being at the opposite side of the unbalanced component. This means that the system is working as well as possible when overloaded.

It is also possible to get a system where stability depends on the amount of imbalance. This can be accomplished by lowering the damping acting on the correction masses. In figure 5.4 three regions are unstable when we lower δ_1 to 0.0007. For low amount of imbalance, m about 0.002, it does not exist any stable equilibrium. The case for m about 0.02 is somewhat better since there exist stable equilibrium for β_3 is some intervals. What might happen in a real system when starting in region 2 and 3 is that the correction masses might move outside the unstable region and stabilize in a stable region. This is somewhat supported by numerical simulations. However, this behaviour is not guaranteed.

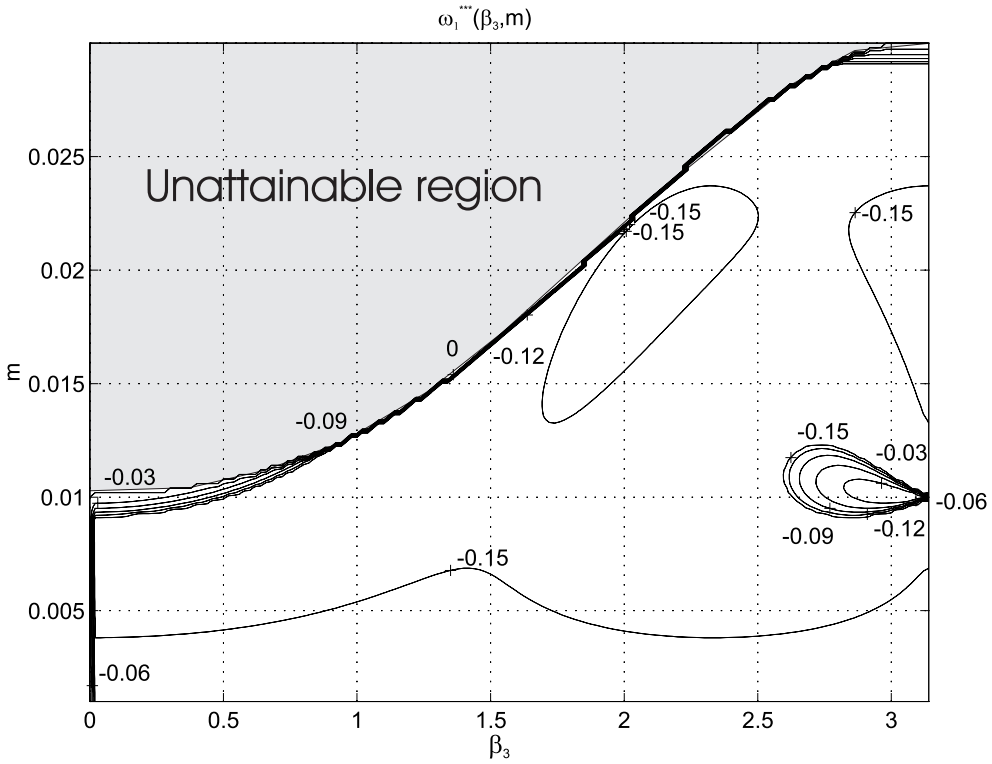

Figure 5.2: Contour plot of stability ω_1^{***} when m is varied from 0 to 0.3 and β_3 in the range 0 to the value given by equality in 5.4. Parameters from table 5.1.

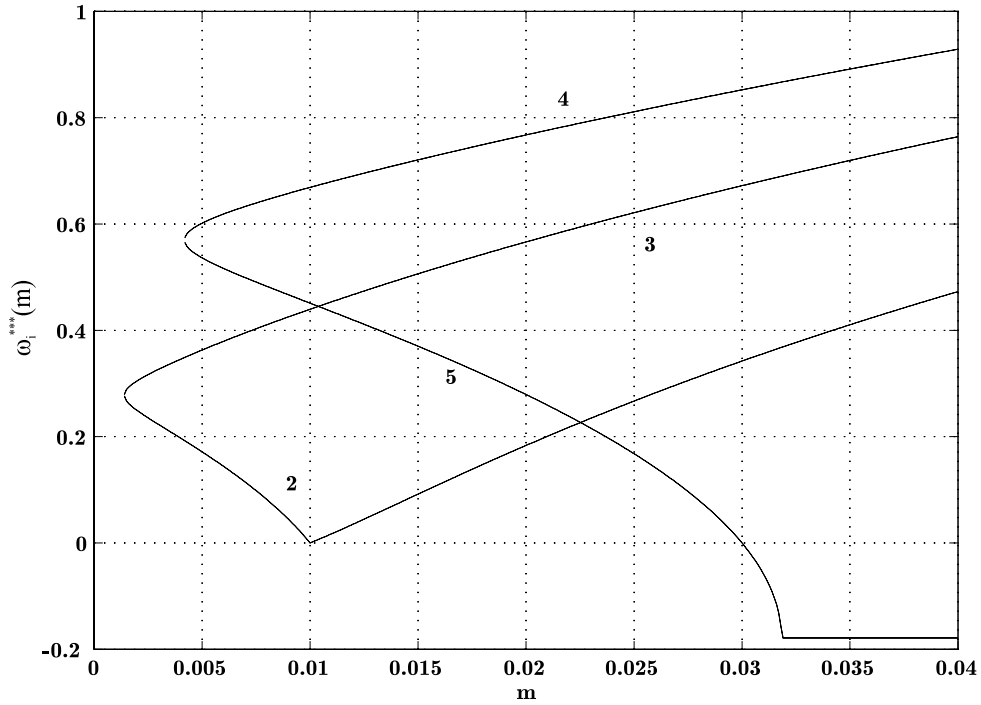

Figure 5.3: Plot of $\omega_{2..5}^{***}$when m is varied from 0 to 0.4. Equilibrium position five become stable when m is above 0.3, which is the maximum amount of unbalance the system can correct for. This means that the system work as well as possible when overloaded. Parameters from tabel 5.1.

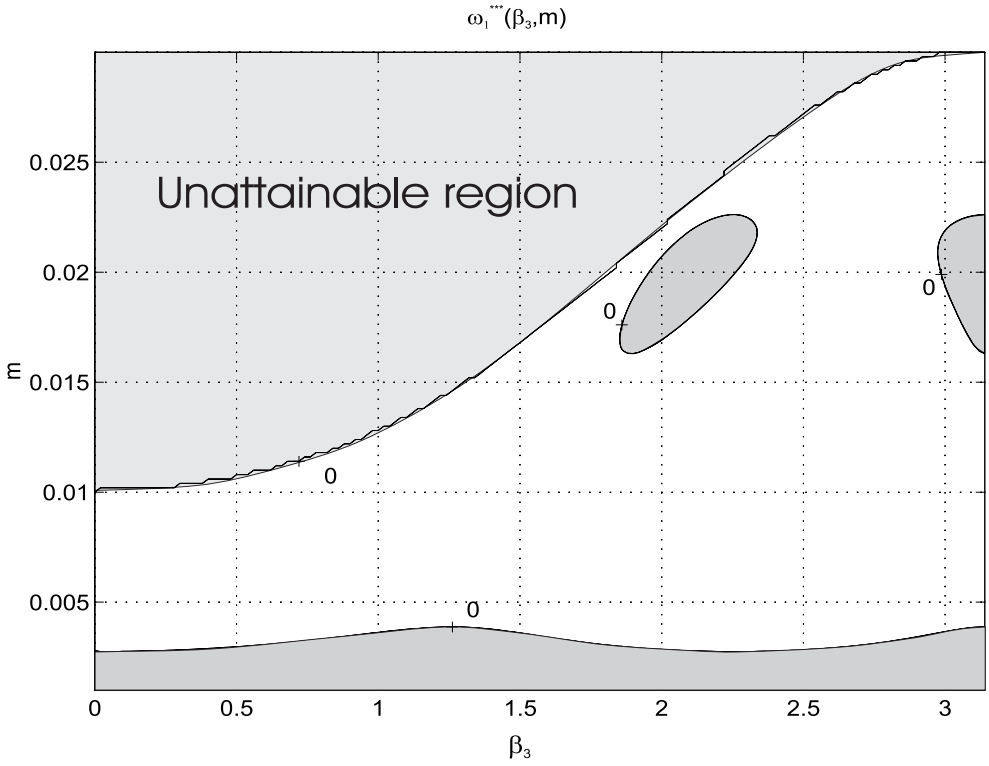

Figure 5.4: Contour plot of the stability when m is varied from 0 to 0.3 and β_3 in the range 0 to the value given by equality in 5.4. Parameters from table 5.1 except for the damping acting on the correction masses, δ_1=0.0007. The dashed area are unattainable, see inequality 5.4. The dark grey area is unstable.

Chapter 6

Conclusions

This analysis has mainly been concerned with local stability analysis. One of the most important conclusions that one can draw from local analysis is that the natural frequency is not the border between stable and unstable balancing operations. However, it seems like running the autobalancer above the natural frequency is a necessary condition for stability.

The local analysis also tells us that the unbalanced equilibrium positions found in the isotropic case are not in general stable in regimes where the balanced equilibrium is stable. This would assure, for example in a system where the unbalance suddenly changes, that the correction masses would not move to an unbalanced equilibrium. The anisotropic case do not show these unbalanced equilibriums.

Another important conclusion is that the autobalancer work as well as possible when overloaded, i.e. all correction masses end up in a stable configuration at the opposite side of the unbalanced component.

This analysis also tells us something about the effects of internal damping compared to external damping. If we have high external[1] damping and low internal damping the autobalancer might be unstable. This effect is particularly noticeable when using two correction masses situated at an angle $\pm\frac{3\pi}{4}$ radians from the line connecting the geometrical centre and the centre of mass of the unbalanced component. This unstability results in a periodic motion of the compensating masses about the balanced equilibrium position.

The anisotropic case, where we have a different spring constant and damping constant in the horizontal and vertical direction, shows a somewhat more complicated stability when the rotational speed is varied. We might then have, depending on the magnitude of separation in horizontal and vertical

[1]The damping from dampers are referred to as external damping and internal damping is the damping acting on the correction masses.

direction, alternating unstable and stable regions when the rotational speed is varied.

It is also shown that it is possible to extend this local stability analysis when more than two correction masses are used. However, we will then have indifferent equilibrium positions. The same instabilities show up in the multiple correction mass case, such as unstabillity due to low internal/high external damping and stability depending on the amount of unbalance.

Although local analysis does not tell what happens when the dynamics are far from the equilibrium position there seems to be a correspondence between the complete dynamics and the local dynamics. This is supported by the numerical simulations. It therefore seems possible to use local analysis for guidance when designing an autobalancing system.

Chapter 7

Acknowledgments

I would like to thank professor Martin Lesser for his support and guidance of this work. Without the Sophia code this work had been almost impossible.

I would also like to thank PhD Arne Nordmark for the time he has spent answering questions and explaining things to me about nonlinear dynamics.

I would also like to thank Anders Lennartsson for using his routines that export Maple code to optimized Matlab code and all the rest of the people at the Department of Mechanics for their interest and suggestions.

Electrolux Research and Innovation let me use my research results obtained while working there and lent us the experimental auto balancer that I built as a part of this work.

Finally I would like to thank the Volvo Research Foundation's mechatronics grant that helped support this research.

Chapter 8

Appendix

8.1 Appendix A

8.2 Solution of equation 3.15

Equation 3.15 can be written as two equations,

$$(k - \omega^2 M')me\sin(\beta_1) + c\omega me\cos(\beta_1) + 2c\omega m_1 l_1 = 0 \tag{8.1}$$

and,

$$\sin(\beta_1)^2 + \cos(\beta_1)^2 = 1 \tag{8.2}$$

to get two well defined solutions. The solution can be written as,

$$\cos(\beta_1) = \frac{-bc \pm \sqrt{a^4 - a^2(b^2 - c^2))}}{a^2 + b^2} \tag{8.3}$$

and,

$$\sin(\beta_1) = \frac{-b\cos(\beta_1) - c}{a} \tag{8.4}$$

where,

$$\begin{aligned} a &= me(k - \omega M')^2 \\ b &= mec\omega \\ c &= 2c\omega m_1 l_1 \end{aligned} \tag{8.5}$$

Bibliography

[1] Jesper Adolfsson. Self balancing of rotating machines: An experimental and theoretical study. Master's thesis, Royal Institute of Technology, Stockholm, Sweden, March 1995. TRITA-MEK, Technical Report 1995:6, ISSN 0384-467X.

[2] V. I. Kravchenko. Stability analysis of a row-type counterbalance. *Mashinovedenie*, (1):25–27, 1983.

[3] V. I. Kravchenko. Automatic balancing of rotor of multi-mass system with row-type automatic ball balancer. *Mashinovedenie*, (2):95–99, 1986.

[4] V. I. Kravchenko, V. A. Manevich, and A. A. Gusarov. Improving the dynamic reliability of loaded machinery elements by self balancing. *Tyazheloe Mashinostoenie*, (5):19–21, 1991.

[5] Martin Lesser. *The Analysis of Complex Nonlinear Mechanical Systems, A Computer Algebra Assisted Approach.* World Scientific, Singapore, to appear in 1995.

[6] Steven H. Strogatz. *Nonlinear Dynamics and Chaos.* Addison Wesley, 1995. ISBN 0-201-54344-3.

[7] William T. Thomson. *Theory of Vibration with Applications, 2nd edition.* Prentice Hall, 1981.